Thesis for the degree of Doctor of Philosophy

# Multi-scale fabric evolution during hydro-mechanical probing of fine-grained soils

Georgios Birmpilis


Department of Architecture and Civil Engineering
CHALMERS UNIVERSITY OF TECHNOLOGY
Göteborg, Sweden 2020

Multi-scale fabric evolution during hydro-mechanical probing of fine-grained soils
Georgios Birmpilis
ISBN 978-91-7905-361-1



Doktorsavhandlingar vid Chalmers tekniska högskola
Ny serie nr 4828
ISSN 0346-718X

Department of Architecture and Civil Engineering
Chalmers University of Technology
SE–412 96 Göteborg, Sweden
Telephone + 46 (0) 31 – 772 1000

Cover image: Observations of natural clay fabric across several length scales ranging from nm observations using X-ray Scattering to mm scale 3D deformations from X-ray Computed Tomography.

Typeset by the author using LaTeX.

Printed by Chalmers Reproservice
Göteborg, Sweden 2020

"Are you looking for the ultimate laws of physics? No, I'm not. I'm just looking to find out more about the world and if it turns out there is a simple ultimate law which explains everything, so be it; that would be very nice to discover. If it turns out it's like an onion with millions of layers and we're just sick and tired of looking at the layers, then that's the way it is. My interest in science is to simply find out more about the world. You see, one thing is, I can live with doubt and uncertainty and not knowing. I think it's much more interesting to live not knowing than to have answers which might be wrong. I have approximate answers and possible beliefs and different degrees of certainty about different things, but I'm not absolutely sure of anything and there are many things I don't know anything about, such as whether it means anything to ask why we're here, and what the question might mean. I might think about it a little bit and if I can't figure it out, then I go on to something else, but I don't have to know an answer, I don't feel frightened by not knowing things, by being lost in a mysterious universe without having any purpose, which is the way it really is so far as I can tell. It doesn't frighten me."

Richard Phillips Feynman

# Abstract

The majority of the studies on sensitive clays so far have focused on the hydro-mechanical response at engineering scale, using concepts from continuum mechanics. The fundamental mechanisms at particle scale, underpinning the emerging response, have so far been studied with *post mortem* analyses. Recent technological advances offer the possibility to monitor the evolving internal material response of clays simultaneously during testing. As opposed to only characterisation of clays at the nanometre scale, in this thesis X-ray techniques were used for a Swedish sensitive clay *in-operando*, during geomechanical testing. The aim was to quantify the response of sensitive clays, spanning from intraparticle to continuum scale, enabling to link the evolving internal material behaviour to the constitutive response at boundary value level. At submicron length-scale, Wide and Small Angle X-ray Scattering at laboratory and synchrotron facilities were used to track particle rotation and intraparticle spacing. This required the development of a plane strain X-ray transparent oedometer cell. X-ray Computed Tomography (XCT) was used to uniquely characterise the undisturbed sensitive clay at submicron scale using a nanotomograph at a synchrotron beam line in 3D. Most importantly, the 4D evolution of internal deformation was quantitatively monitored during drained hydro-mechanical probing. The latter required the development of XCLAY, a bespoke miniature Bishop-Wesley triaxial cell enabling advanced stress-path testing compatible with XCT. X-ray scattering provided insight on the nanometre scale, in terms of the integrated response of intraparticle strain and particle orientation. During the 1D compression test two minerals present in the natural clay behaved differently: illite was stable, while for montmorillonite a new spacing was detected. Both minerals continued to align towards the horizontal axis. For the first time, the internal 3D structure within an undisturbed sensitive clay sample was revealed at submicron scale. The evolving internal deformations of the natural sensitive clay were resolved during hydro-mechanical probing *in-operando* under drained triaxial compression, considering pseudo-isotropic, $K_0$ and highly deviatoric loading. The 4D deformation fields were extracted from the tomography data using Digital Volume Correlation (DVC). The $K_0$ stress path resulted in the most homogeneous full-field strain maps, while the highly deviatoric path resulted in very inhomogeneous strain fields. The mean values of the strain fields compared well with the external measurements, thereby reinforcing the validity of prior experimental data on soft clays. The thesis demonstrates that geomechanical laboratory tests on fine-grained soils can be elegantly combined with non-destructive techniques.

**Keywords:** sensitive clays, X-ray Scattering, X-ray Computed Tomography, geomechanical testing, clay fabric

# Acknowledgments

The PhD project was financially supported by the Swedish Research Council (Vetenskapsrådet) and the Swedish Transport Administration (Trafikverket). Their contribution is greatly appreciated by the author. Furthermore, significant part of the experimental work was conducted in synchtrotron facilities: MAX-lab, Sweden, and the European Synchrotron Radiation Facility (ESRF), France, that are greatly acknowledged for the granted beamtime and the support provided by their personnel.

The everyday reality behind all the figures and data of this thesis, however, consists of hard work of a group of people and so many personal moments shared among friends and colleagues. Therefore, I need to express my gratitude to all the persons that shared this trip with me.

I would like to first thank my supervisors: Jelke Dijkstra, Mats Karlsson and Stephen Hall. I would like to honestly thank Mats for his patience to my curiosity and for sharing his expertise in the lab through our discussions, and Stephen for introducing me in the world of non-invasive testing of geomaterials. The greatest "Thank you" for this work can only go to Jelke who was the main supervisor, but also a mentor for me all through these years. Jelke, you helped me to develop and expand my horizons as researcher with your guidance, but also by giving me space and confidence to raise my research quests to any direction I saw fit. I would also like to thank Minna Karstunen for her support, trust and her role as the examiner of this thesis. Furthermore, I am thankful to the good friends in Laboratoire 3SR in Grenoble, Eddy and Olga, for their hospitality and help during my visit there. Special thanks goes also to Aaro Pirhonen and Anders Karlsson. Without their craftsmanship it would be impossible to turn all the crazy ideas to small -still crazy- devices, essential for this doctoral thesis: Ett stort och varmt tack till er!

All through these five years, I had the pleasure to work with so many interesting people, make new friends and I am grateful to all my colleagues that we shared long days, exciting trips, interesting discussions and fun parties together. I hope that we will keep having even more exciting moments in the future.

A unique place in my heart is saved for my closest friends. Together we have shared all these years away from home, even though we are scattered around the world. These friends that you are allowed to complain to, make fun of, argue with about anything and everything and celebrate the greatest moments in life together.

Last but not least, I want to dedicate this thesis to my family in Greece, that I have missed much during these years. They have shaped me to the person I am today and provided all the available means to help me take my own path in life.

Georgios Birmpilis
Göteborg, September 2020

# List of Publications

This dissertation is a compilation thesis and consists of two parts. Part A consists of introductory chapters that navigate the reader through the topic and puts the appended papers into context. Part B contains the appended papers:

**Paper I.** Birmpilis, G., Ahmadi-Naghadeh, R. & Dijkstra, J. (2019). Towards a methodology for the characterisation of the fabric of wet clays using X-ray scattering.*7th International Symposium on Deformation Characteristics of Geomaterials (IS-Glasgow 2019)*, 26-28 Jun 2019, Glasgow, E3S Web Conf, Volume 92, EDP Sciences.

**Paper II.** Birmpilis, G., Ahmadi-Naghadeh, R. & Dijkstra, J. (2019). Macroscopic interpretation of nano-scale scattering data in clay. *Géotechnique Letters*, 9(4), 355-360. Themed issue on 'Micro to Macro Mechanics'.

**Paper III.** Birmpilis, G., Hall, S.A., Lages, S. & Dijkstra, J. (2019). Monitoring of the nano-structure response of natural clay under mechanical perturbation using small angle X-ray scattering and digital image correlation. *Acta Geotechnica 14*, 1965–1975.

**Paper IV.** Birmpilis, G., Andò, E., Stamati, O., Hall, S.A., Gerolymatou, E. & Dijkstra, J. (2020). Experimental quantification of 3D deformations in sensitive clay during stress-probing. Manuscript.

**Own contribution**
The author of this thesis has carried the main responsibility for the work presented in this dissertation and the writing of the appended papers. The design of the experimental equipment in Papers III & IV was also mainly developed by the author. Experimental preparations, data analysis and review of the appended publications was conducted by the author in collaboration with the co-authors.

**Other publications**
During this research project, additional publications relevant to the topic were published by the author:

- Birmpilis, G., Dijkstra, J. & Hall, S.A. (2016). Miniature sampling method in experimental geomechanics for soft soils. *Proceedings of the 17th international conference on experimental mechanics (ICEM 17)*, 3-7 July 2016, Rhodes, Greece.

- Birmpilis, G., Dijkstra, J., Tudisco, E., & Hall, S.A. (2017). In-situ study of deformation mechanisms of soft clay using X-ray Computed Tomography and Digital Volumetric Correlation. *3rd International Conference on Tomography of Materials and Structures*. 26-30 June 2017, Lund, Sweden, ICTMS2017-30 (2017).

- Birmpilis, G., Nordin, M. & Dijkstra, J. (2018). Numerical Scattering Experiments on Assemblies of Clay Platelets. *In: Giovine P., Mariano P., Mortara G. (eds) Micro to MACRO Mathematical Modelling in Soil Mechanics*. Trends in Mathematics. Birkhäuser, Cham.

# List of Acronyms

**CCD** Charged-Coupled Device. 34

**CEC** Cation Exchange Capacity. 9, 10

**DDL** Diffuse Double Layer. 15, 16

**DIC** Digital Image Correlation. xvi, 27, 28, 36, 37

**DVC** Digital Volume Correlation. v, 34, 37, 38, 42

**EM** Electron Microscopy. 4

**FoV** Field of View. 29

**MD** Molecular Dynamics. 16

**MIP** Mercury Intrusion Porosimetry. 4, 14, 15, 21

**PID** Proportional–Integral–Derivative. 33

**SAXS** Small Angle X-ray Scattering. 24–27

**SEM** Scanning Electron Microscopy. xv, 8, 12–15, 21

**USAXS** Ultra Small Angle X-ray Scattering. 24

**WAXS** Wide Angle X-ray Scattering. 24, 26

**XCT** X-ray Computed Tomography. 5, 29, 34, 35, 41, 42

**XRD** X-ray Diffraction. 4, 8, 14, 42

# Nomenclature

| | |
|---|---|
| $2\theta$ | scattering angle |
| $\beta$ | absorption index |
| $\delta$ | refractive-index increment |
| $\eta$ | ratio of deviatoric to mean effective stress |
| $\lambda$ | radiation wavelength |
| $\mu$ | linear attenuation attenuation coefficient |
| $\omega$ | angular frequency |
| $\varepsilon_d$ | deviatoric strain |
| $\varepsilon_v$ | volumetric strain |
| $d$ | d-spacing |
| $E$ | electric field vector |
| $e$ | Euler's number |
| $e$ | void ratio |
| $E_0$ | electric field vector amplitude |
| $I$ | intensity of electromagnetic radiation |
| $i$ | imaginary unit |
| $I_0$ | intensity of electromagnetic radiation amplitude |
| $k_0$ | angular wavenumber |
| $M$ | critical state slope |
| $n$ | refractive index |
| $p'$ | mean effective stress |
| $q$ | deviatoric stress |

| | |
|---|---|
| $q$ | scattering vector |
| $S_t$ | sensitivity |
| $S_u$ | intact undrained shear strength |
| $S_{ur}$ | remoulded undrained shear strenght |
| $t$ | time |
| $w_t$ | natural water content |
| $x$ | position in wave propagation direction |

# List of Figures

# List of Tables

# Contents

# Part A

# Extended Summary

# Chapter 1

# Introduction

## 1.1 Background

A large part of the population lives in densely populated urban areas in proximity to the coast, lakes and other waterways, *e.g.*, Small and Nicholls (2003). This global population trend is corroborated in Nordic countries, such as Sweden (Svanström, 2012). The areas in Sweden with the highest population density also have the largest risk for flooding and landslides (Nadim et al., 2008). In Sweden, major incidents of quick clay landslides have been recorded for example in Surte (1952) and Tuve (1977), see Figure 1.1, causing fatalities and large economic losses. The susceptibility for landslides is directly linked to the abundance of soft soil deposits of marine origin that have unfavourable engineering properties. The relatively high strength and stiffness of sensitive clays when intact, compared to other normally consolidated natural soft clays, subsequently suddenly degrades, when disturbed or excessively loaded.

In Southwestern Sweden large areas of sensitive clay are deposited resulting from a complex geological history (Bergsten, 1994). These deep deposits of sensitive clay pose geotechnical engineering challenges, whilst the societal demands on safety and urban densification are increased. This has resulted in unique engineering challenges in soft soil areas related to slope stability (Petterson, 1955; Larsson and Jansson, 1982; L'Heureux et al., 2011), deep foundations (Wood and Karstunen, 2017), excavations (Hashash and Whittle, 1996) and line infrastructure (Karstunen and Yin, 2015; Amavasai et al., 2018).

The majority of the scientific advances in studies on sensitive clays have focused on the emerging hydro-mechanical response at engineering scale, using concepts from continuum mechanics. In this approach the material is modelled as a continuum, with a constitutive law that relates an increment of strain (or stress) to an increment of stress (or strain). Over the years, a large number of continuum models have been developed to capture the response of natural clays with increasing fidelity, eg., Pestana and Whittle (1999), Rouainia and Muir Wood (2000), Gajo and Muir Wood (2001), Wheeler et al. (2003), Karstunen et al. (2005), Grimstad et al. (2010), Yin et al. (2011), Sivasithamparam et al. (2015), and Gras et al. (2018). These models often

Figure 1.1: Tuve landslide (Gothenburg, Sweden, 1977) total damage costs are estimated to 140 million SEK ($\sim$ 14 million €), source: en.wikipedia.org.

incorporate intricate hardening laws that capture the effects of complex non-linear irreversible mechanisms originating at the particle scale.

In absence of experimental data on the 3D deformations within a soil sample, these hardening laws are calibrated at continuum level using data from hydro-mechanical laboratory tests using measurements on the boundary of the sample. Nevertheless, element testing is unavoidably biased by the boundary conditions of the experiment, the sample quality and the size of the representative elementary volume. Several examples on the limitations of a conventional triaxial test, a common advanced laboratory test to quantify the hydro-mechanical response of clay samples at continuum scale, are discussed by Donaghe et al. (1988). Simultaneously, technological advances in Clay Science have provided revolutionary understanding of fundamental clay behaviour through electron microscopy and diffraction techniques. Clay particles and their composition have mainly been studied on the (intra)particle scale, without directly linking it to the emerging mechanical response at the continuum scale (Grim, 1953; Brindley and Kurtosi, 1962; Bohor and Hughes, 1971). The preparation of the material for subsequent testing, however, fixes the state, and is still rather invasive to the material structure (Gillot, 1970; Deirieh, 2016).

Some of the advanced experimental characterisation techniques have subsequently been employed within geomechanics, where classic geomechanical testing at the continuum scale is combined with *post-mortem* characterisation of samples using X-ray Diffraction (XRD), Electron Microscopy (EM) or Mercury Intrusion Porosimetry (MIP) (Quigley and Thompson, 1966; Lambe and Whitman, 1969; Diamond, 1970; Martin and Lad, 1975; Delage and Lefebvre, 1984; Cotecchia and Chandler, 1997; Iñigo et al., 2000; Tarantino and De Col, 2008; Hattab and Fleureau, 2010; Hattab et al., 2013) . These results illustrate the importance of capturing the evolving microstructure during mechanical loading, and its impact on the subsequent strain increment. However, due to the preparation requirements, these experimental

methodologies are still unable to capture the evolving response, as after retrieving samples for further advanced material analyses, the geomechanical test is aborted.

Recent technological advances, such as non-invasive techniques, offer the possibility to examine the internal material response of the soil during an element test both at continuum and particulate level. The natural contrast in some rocks and coarse grained materials, such as sands, enables the quantification of the internal kinematics during a geomechanical tests using time-resolved X-ray Computed Tomography (XCT) and digital image correlation (Lenoir et al., 2007; Alshibli and Hasan, 2008; Matsushima et al., 2010; Hall et al., 2010; Andò et al., 2012). Especially the rich contrast in the density between the grains and the pores, as well as the relatively large grain size (0.2 - 1 mm) makes sand an ideal material for these kind of studies, with respect to the typically micrometre voxel size achieved (Andò, 2013). These type of studies have not been reported for (natural or reconstituted) clays.

Models based on fundamental laws for material behaviour starting from the observations at the micro-scale potentially can improve the hardening laws in the current phenomenological continuum models. Additionally, a deeper understanding of inner structure of the material can inform strategies to improve the mechanical response at the engineering scale, hence mitigating the geotechnical problems associated with sensitive clays.

## 1.2 Aims & objectives

The aim of this research is to quantify the behaviour of natural sensitive clays under hydro-mechanical loading, by investigating the response using X-ray based scattering and imaging techniques. Therefore, quantified measurements of deformations at several length scales (nm - cm) will be pursued. The focus will be on linking the evolving internal material behaviour to the constitutive response at boundary value level using advanced geotechnical test control. Thus, the results directly aid the development of advanced constitutive models for natural sensitive clays. In parallel, this work aims to validate the boundary value interpretation that is currently in use for the interpretation of geotechnical element tests on sensitive natural clays.
The following objectives are formulated:

- To identify non-intrusive (quasi) real-time measurement techniques to investigate sensitive clays in their natural (saturated) state, in order to capture the evolving mechanisms of the rate-dependent material response.

- To develop bespoke versatile apparatuses for geomechanical testing, whilst being compatible with advanced X-ray based measurement techniques at large testing facilities.

- To advance element level testing of soils by incorporating the latest developments in mechatronics into the geotechnical laboratory, thereby enabling test miniaturisation, automation and subsequent parallelisation.

## 1.3 Limitations

During the last decade, availability to X-ray facilities has rapidly improved. Nonetheless, these kind of techniques are still not readily accessible for everyday laboratory testing. Thus, the amount of experimental data presented herein remains modest, when compared to traditional experimental studies in geomechanics. Whilst great advances have been made for the characterisation of stress in coarse grained geomaterials, that are frictional materials, by measuring the strain in the crystal lattice of the grains (Hall et al., 2018), analogous techniques have not yet been developed for fine-grained geomaterials.

## 1.4 Main research contributions

The main research contributions of this thesis can be summarised as:

- Characterisation of a natural sensitive clay in its natural undisturbed state (Paper I, Paper III, Section 3.3 in the extended summary);
- Development of miniature geomechanical test equipment that facilitates monitoring of the internal response in clay samples using X-ray based measurement techniques. Most notably, these include the plane-strain compression cell for scattering (Paper III) and the miniature triaxial cell for advanced stress path probing of soft clays (Paper IV);
- The quantification of the evolution of fabric changes in intact specimens of natural sensitive clay, using *in-operando* experiments. These measurements span from intraparticle (nm) (Paper II & III) to engineering scale (cm) (Paper IV), correlating the emerging hydro-mechanical response of the material to the changes of the constituents and its 3D structure.

# Chapter 2

# Natural fine-grained soils

Natural deposits of fine-grained soils are complex mixtures of clay and non-clay particles at a non-isotropic stress state. The physico-chemical properties and the frictional response of larger particles contribute to the emerging hydro-mechanical behaviour of the material at the engineering scale. In this Chapter, firstly the components of the soil structure are elaborated from atomic to inter-particle scale, following the hierarchical system of clay structure. Subsequently, the resulting macroscopic hydro-mechanical behaviour is discussed. An illustration of this hierarchy is shown in Figure 2.1. Up to particle level, clay consists of almost perfect, crystal structures. The particles are dispersed in water forming a colloidal system with much higher degree of disorder that governs the emerging hydro-mechanical response at engineering scale. Each of the structures, as well as the governing mechanisms, will be elaborated from a geomechanical perspective and serves a background for the research conducted in this thesis without aiming it to be exhaustive.

## 2.1 Clay fundamentals

In geotechnical engineering clay is, incompletely, classified by particle size and class of minerals. Particles with sizes up to 2 µm are classified as the clay fraction (EN ISO 14688-1, 2017). The type of mineral is distinguished from the net negative electrical charge, plasticity (Atterberg, 1911; Casagrande, 1932; White, 1949; Seed et al., 1966) and high weathering resistance (Mitchell and Soga, 2005). The minerals in natural clay deposits are primarily hydrous aluminium silicates. There is no rigorous link between the constituents of the clay and the emerging engineering properties, such as strength and stiffness, as this is affected by the arrangement and shape of the particles and the inter-particle interaction potentials. All of these depend on the physico-chemical environment in which the clay particles are created, deposited and consolidated.

### 2.1.1 Clay Crystals

Clay particles consist of a crystal structure. The structure of the crystal lattice and the subsequent classification of clay mineral groups, based on their composition,

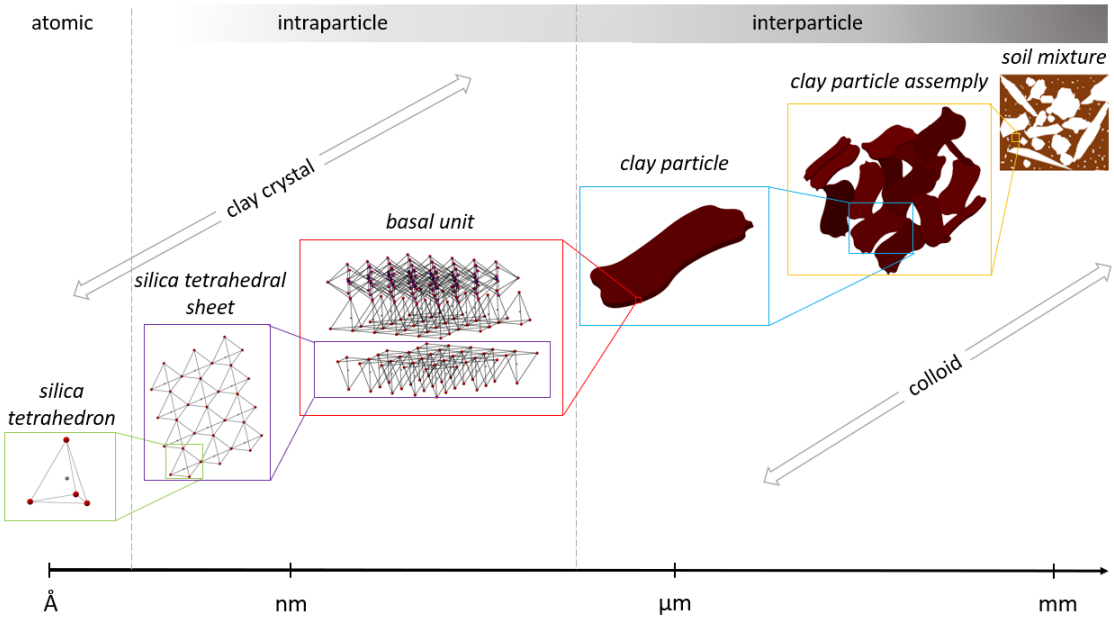


Figure 2.1: Schematic representation of the hierarchical structure of clay from atomic to inter-particle scale.

was made possible by the combined use of XRD and SEM (Grim, 1953). Clay minerals have a layered structure. Different combinations of sheets of silica tetrahedra, $SiO_4^{4-}$, and aluminium (or magnesium) octahedra, $Al(OH)_6^{3-}$, (Figure 2.2) compose different clay types. Differences among minerals within the clay mineral groups result primarily from differences in the type and amount of isomorphous substitution within the crystal structure. Possible substitutions are nearly endless in number, and the crystal structure arrangement may range from very poor to nearly perfect (Mitchell and Soga, 2005).

In Figure 2.3 the schematic representation of four types of basal units is presented. Silica sheets are formed by tetrahedrons interconnected in the same plane with composition $(Si_4O_{10})^{4-}$ and can repeat indefinitely. The octahedral sheet structure is composed of magnesium or aluminium in octahedral coordination with oxygen or hydroxyl. If the cation is trivalent, *e.g.*, $Al^{3+}$, then normally only 2/3 of the possible cationic spaces are filled, and the structure is termed dioctahedral. This composition and structure forms the mineral gibbsite. If the octahedrally coordinated cation is divalent, *e.g.*, $Mg^{2+}$, then normally all possible cation sites are occupied and the structure is trioctahedral giving the mineral brucite. The synthesis pattern that is produced by different possible stackings of basal units is responsible for the type of clay mineral formed (Figure 2.4). The bonds in clay minerals are primary bonds, typically half ionic and half covalent (Mitchell and Soga, 2005).

### Isomorphous substitution

The wide range of different clay compositions is due to isomorphous substitution, *i.e.*, the exchange of cations of similar size and valence, while the crystal structure is

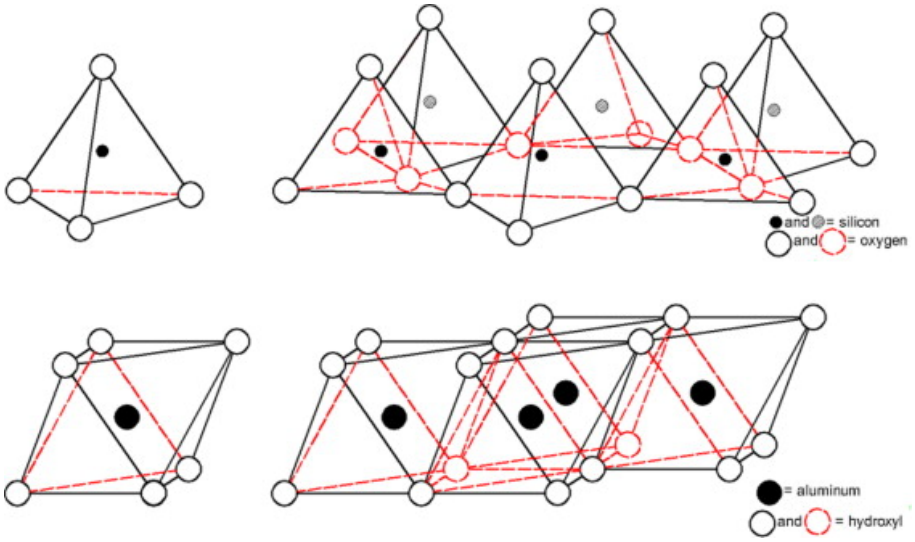


Figure 2.2: Structure of a silica tetrahedral sheet (top: black dots represent silica and white dots represent oxygen atoms) and an alumina octahedral sheet (bottom: black dots represent aluminium or magnesium and white dots represent hydroxyl units) (Davalos et al., 2012).

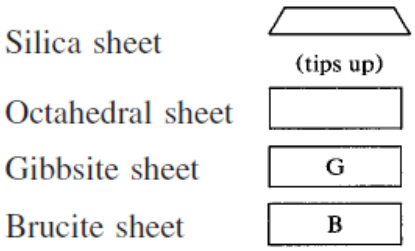


Figure 2.3: Schematic representations of basal unit sheets.(Mitchell and Soga, 2005).

preserved. This process is completed during the formation of minerals and is the factor that determines the permanent charge of the mineral, and thus its Cation Exchange Capacity (CEC). In an ideal brucite sheet, all the octahedral spaces are filled by magnesium. In an ideal silica sheet, silicons occupy all tetrahedral spaces. In clay minerals, however, some of the tetrahedral and octahedral spaces are substituted by other cations compared to the ideal structure. Common examples are aluminium in place of silicon, magnesium instead of aluminium, and ferrous iron $Fe^{2+}$ for magnesium. Isomorphous substitution in most clay minerals gives clay particles a net negative charge.

### Clay subgroups

There is a great variety of clay types found in natural clay deposits formed by consolidation, with large differences in emerging hydro-mechanical behaviour. Three common clay subgroups, however, outline some of the most important clay properties for geotechnical engineering: kaolin, micalike and smectite minerals.

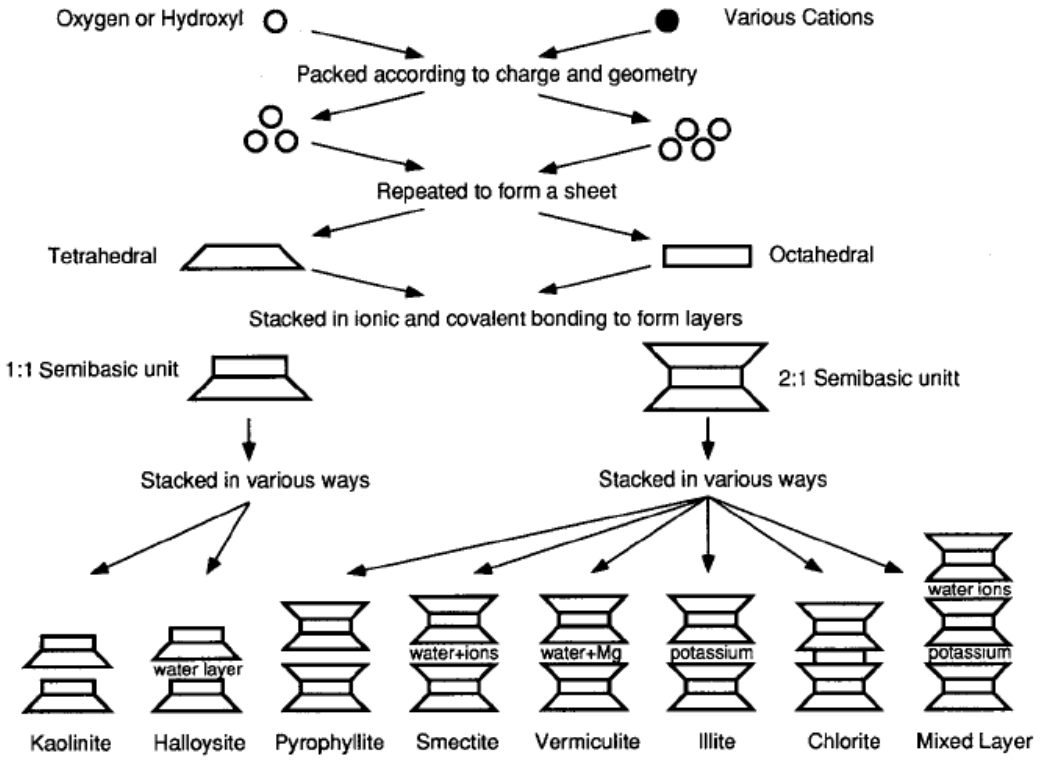


Figure 2.4: Synthesis pattern for the clay minerals.(Mitchell and Soga, 2005).

- Kaolin minerals are composed of alternating silica and octahedral sheets and are thus 1:1 minerals. The group includes the dioctahedral minerals kaolinite, halloysite, dickite, and nacrite, and the trioctahedral minerals chrysotile, antigorite, chamosite, and cronstedite. Probably the most ubiquitous silicate minerals in soils throughout the world are the layer silicates of the kaolin group. The bonding between successive layers is by both van der Waals forces and the hydrogen bonds, creating strong bonds. Additionally, due to the low amount of isomorphic substitutions in kaolin, clay minerals from the kaolin group do not have a permanent charge and thus do not swell in the presence of water (Underwood et al., 2012).

- Illite (commonly referred to as hydrous mica) is a micalike clay mineral. Illite structure is of 2:1 type, dioctahedral, non-expanding, alumininous, and contains non-exchangeable $K^+$ as the major interlayer cation. The potassium balances a negative layer charge, generated by $Al^{3+}$ for Si substitution in the tetrahedral sheet and ($Mg^{2+}$, $Fe^{2+}$) for $Al^{3+}$ in the octahedral sheet (Środoń, 1999).

- The minerals of the smectite group have an original structure consisting of an octahedral sheet sandwiched between two silica sheets. Smectite type minerals are expandable due to extreme isomorphous substitution taking place. Smectite minerals have high CEC, in the range of 80 to 150 meq/100 g (Mitchell and Soga, 2005) and are susceptible changes in surface charge.

In nature, mixed-layer clay minerals are also observed. Interstratification of two or more layer types often occurs within a single particle, due to the great similarity in crystal structure among the different minerals. A typical example is the illite-smecite mixed mineral system (Figure 2.5). A structural abnormality in cases observed of mixed mineral systems is turbostratic disorder. It describes structures in which basal planes have slipped out of alignment (Lutterotti et al., 2010).

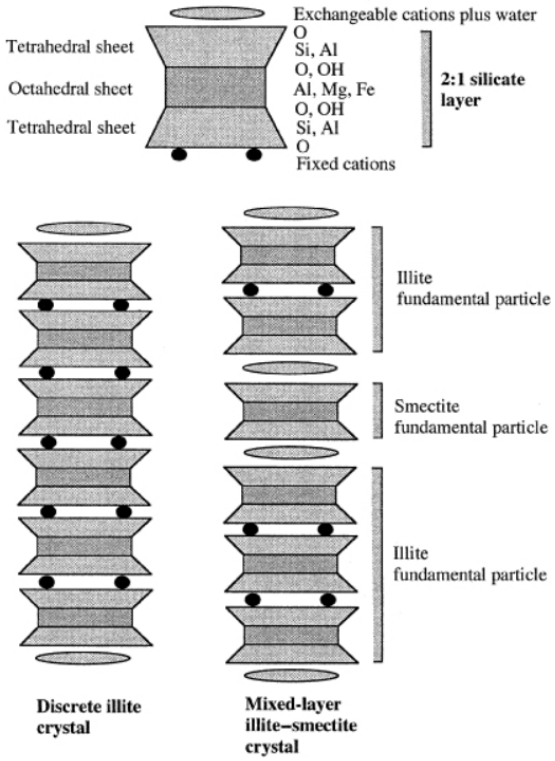


Figure 2.5: Schematic structure of the 2:1 silicate layer in the case of discrete illite crystal (left) and mixed-layered illite-smectite crystal (Środoń, 1999).

### 2.1.2 Clay particles

Clay particles are formed by the aggregation of a large number of basal unit layers. The dimensions of a clay particle can differ depending on its type with dimensions ranging between some hundreds of nanometres length and some nanometres thickness (Nadeau, 1985). A plate-like particle shape is typical for several types of clay, such as kaolinite (hexagonal, Figure 2.6) and montmorillonite (smaller and thinner flakes, Figure 2.8), while some minerals can form tubular particles (e.g., halloysite, Figure 2.7). The aspect ratio is typically around 10 for kaolinite and can reach up to high values ($\sim$500) for smectites (Żbik, 2010).

Clay particles are charged particles generally characterised by a high specific surface. The high specific surface compared to the particle mass and the unsatisfied force equilibrium of the structure at the boundaries of the particle govern the behaviour of the material. An equilibrium is obtained by attraction of molecules of

the surrounding phase, cohesion to similar particles or readjustments of the internal structure (Mitchell and Soga, 2005). The nature of such forces is weaker than the primary bonds in the crystal structure, that are of electrostatic nature, such as van der Waals forces.

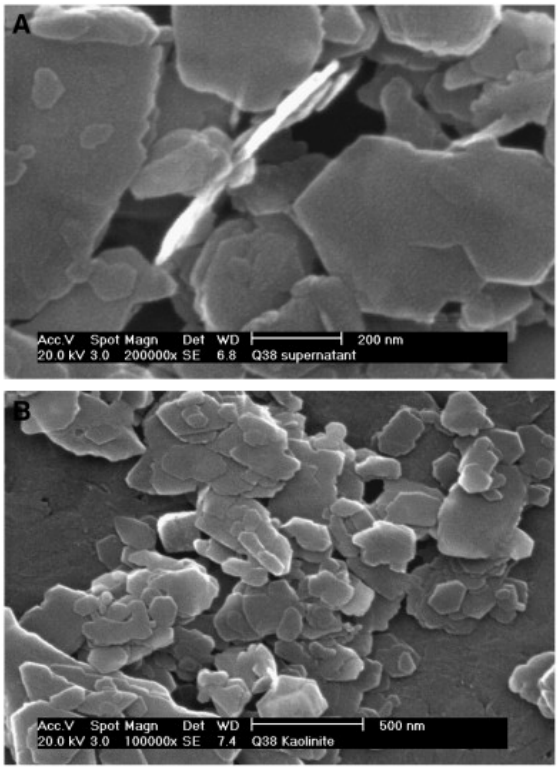


Figure 2.6: SEM micrographs of kaolinite at high magnification (A) and low magnification (B) (Du et al., 2009).

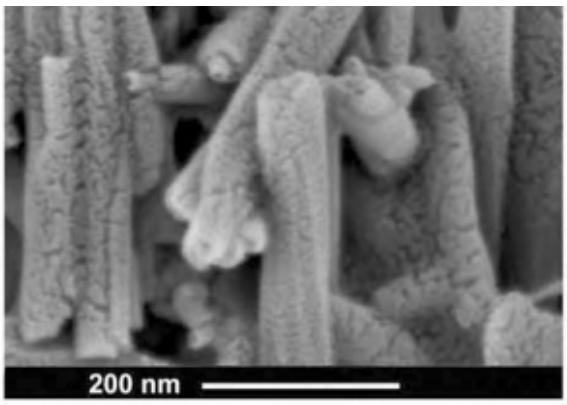


Figure 2.7: Cryo-FE-SEM images showing the original morphology of hydrated halloysite (Işik Ece and Schroeder, 2007).

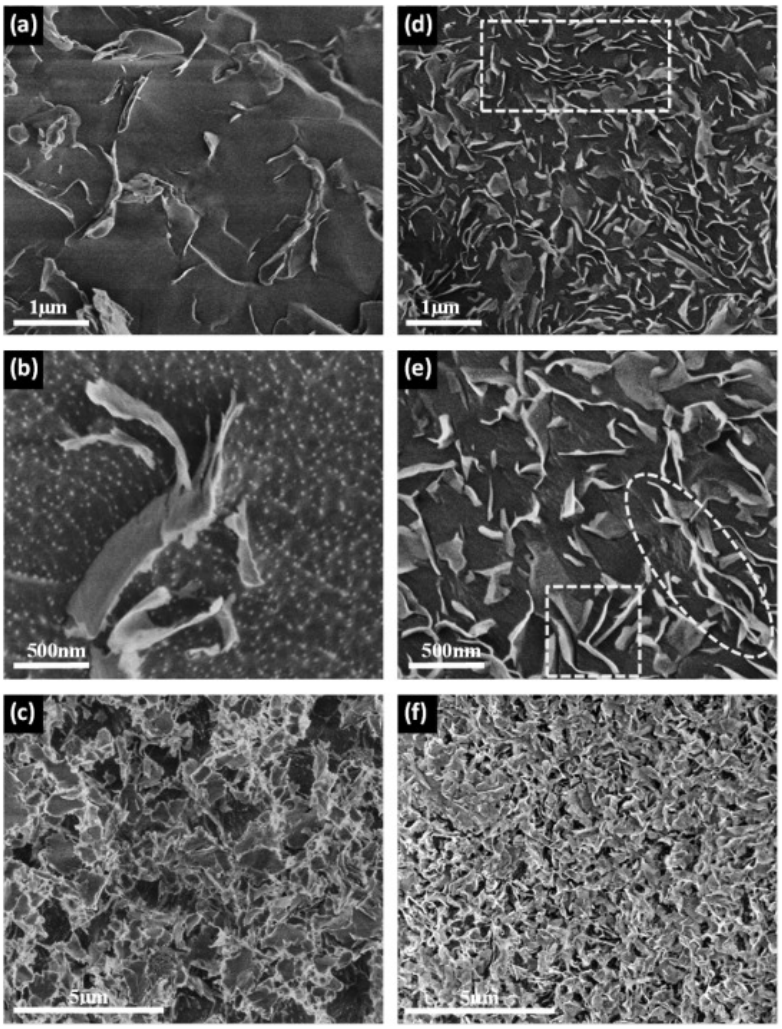


Figure 2.8: Cryo-SEM images of high-pressure frozen and freeze-fractured SWy-2 bentonite in distilled water with 5% (wt/wt) solid content: (a–c) Ca-ion exchanged suspension, and (d–f) Na-ion exchanged gel (Mouzon et al., 2016).

### 2.1.3 Clay fabric

In geotechnics, the geometrical arrangement of clay particles and particle contacts is referred to as clay fabric, while the term structure is describing the interparticle forces in addition to fabric (Lambe and Whitman, 1969; Cotecchia and Chandler, 1997). Several types of possible particle associations in suspensions can be formed during sedimentation. An overview by van Olphen (1964) is presented in Figure 2.9. Similar fabric associations are observed also in natural soils (Collins and McGown, 1974). These structures result from the interaction of clay particles, the aqueous suspension, and the ionic content of the suspension. The plate-like particles have different crystal structures on their edges and faces. Thus, the electrical charges on the particle edges are often different from those on the particle faces. Clay particles interact in edge-to-edge, edge-to-face and face-to-face modes. When the face-to-edge contact dominates, the microstructure is characterised as a house of cards (van Olphen, 1964;

Khandal and T.Tadros, 1988).

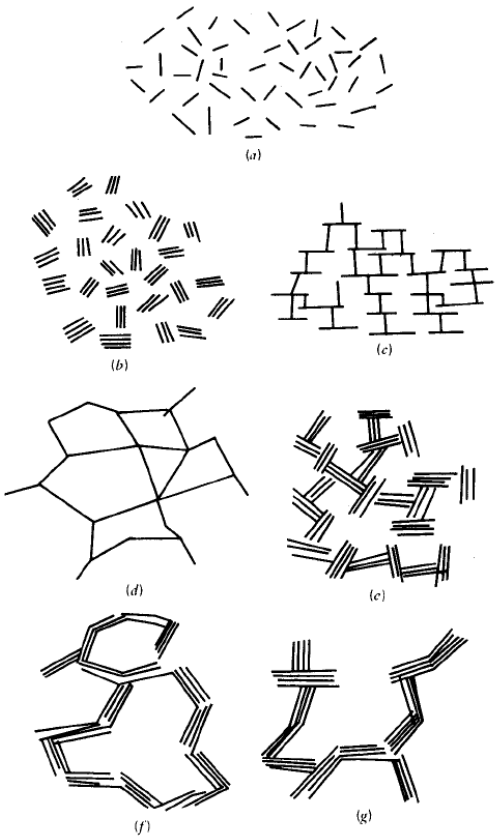


Figure 2.9: Modes of particle associations in clay suspensions and terminology. (a) Dispersed and deflocculated, (b) aggregated but deflocculated (face-to-face association, or parallel or oriented aggregation), (c) edge-to-face flocculated but dispersed, (d) edge-to-edge flocculated but dispersed, (e) edge-to-face flocculated and aggregated, (f) edge-to-edge flocculated and aggregated, and (g) edge-to-face and edge-to-edge flocculated and aggregated (van Olphen, 1964).

Another type of fabric geometry, shown in Figure 2.10, based on ultra microscope observations (a microscope which uses reflected or transmitted light but it provides only the most rudimentary indication of the particle sizes and shapes) for clay suspensions is the honeycomb structure (Ehrenberg, 1918). Subsequently, Terzaghi and Casagrande formulated the "Terzaghi-Casagrande honeycomb structure", which declares that clay minerals stick to each other at points of contact, with forces sufficiently strong to construct a honeycomb structure, which permits large amounts of water to be enclosed within the voids. Each unit or cell of the honeycomb was envisioned as being made up of numerous single grains held together by adhesion (Bennet and Hulbert, 1986).

Fabric has been studied through imaging technics such as SEM, MIP and XRD (Grim, 1953; Diamond, 1970; Bohor and Hughes, 1971; Delage and Lefebvre, 1984; Tarantino and De Col, 2008). Special interest has been on the case of sensitive clays, due to their naturally formed open structure (Quigley and Thompson, 1966; Gillot,

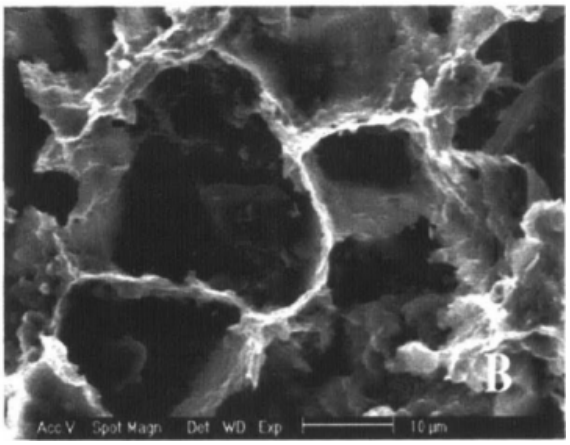


Figure 2.10: Honeycomb fabric of illite through SEM imaging (O'Brien, 1971).

1970; Pusch, 1970; Delage and Lefebvre, 1984). Particle orientation is a parameter that used for tracking fabric changes, as demonstrated by Martin and Lad (1975), Iñigo et al. (2000), DiMasi et al. (2001), Hattab and Fleureau (2010), Hattab et al. (2013), and Cotecchia et al. (2019).

Invasive techniques such as SEM and MIP, however, are biased by the preparation procedure (especially water replacement) resulting not only in volume change (Gillot, 1970) but also in the type of the observed structure. Deirieh (2016) and Deirieh et al. (2018) re-examined the influence of the disturbance of the sample during the preparation stages necessary for microscopy techniques using state-of-the-art technologies. They compared cryo-SEM and conventional SEM techniques, and the results demonstrate that structures such as honeycomb might be artifacts of the preparation technique.

### Double Layer Models

The mechanical behaviour of fine-grained materials is not only determined by the geometrical configuration of the particles (fabric) or mechanical friction, but also by the attraction and repulsion forces in-between the particles. Isomorphous substitution is responsible for the net negative charge in clay particles. When suspended in an electrolyte, clay particles are surrounded by a hydrosphere of adsorbed water that contains a thin layer of adsorbed cations. Outside this layer, ions of opposite polarities form an electrically neutral diffuse layer. The adsorbed cations are influenced by electrostatic attraction. On the other hand, the diffuse layer cations are influenced by opposing forces: electrostatic attraction and diffusive forces. This ionic structure consisting of the negative surface charges, adsorbed cations, and the diffuse layer which is known as the Diffuse Double Layer (DDL). The thickness of the DDL is $<10$ nm (Mojid, 2014). For colloidal systems of electrically charged particles, several models based on double layer theory have been formulated. The first to introduce the concept of the existence of a double layer on a charged surface in contact to an electrolyte was Helmholtz (1879) (Stojek, 2002). This concept is based on the idea that the electrode-electrolyte system acts as a capacitor. Helmholtz layer

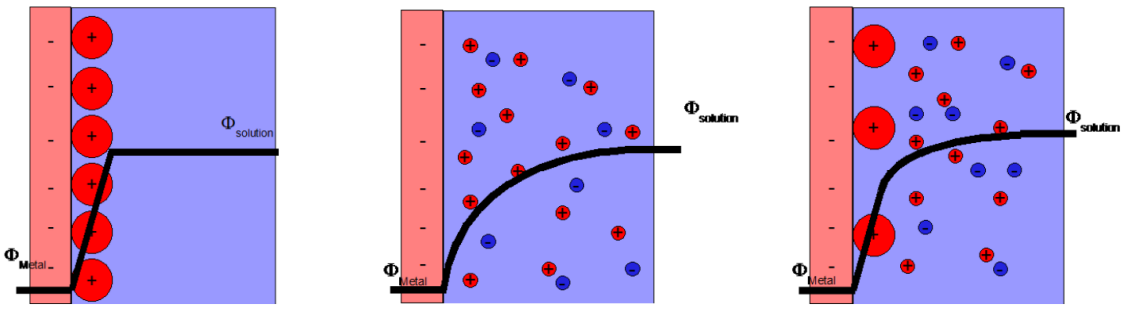


(a) Helmholtz (b) Gouy-Chapman (c) Stern

Figure 2.11: Schematic representation on potential distribution close to the electrode-electrolyte interface by (a) Helmholtz, (b) Gouy-Chapman, and (c) Stern model. (Source www.garmanage.com)

theory had limitations in correlation to experimental data due to the assumption of constant capacitance of the system. Gouy and Chapman (1910) developed this concept adopting a Poisson–Boltzmann ion distribution. In this model a DDL is involved, in which in contrast to the Helmholtz approach, the ions accumulate at a distance from the solid interface. Later in 1924 Stern suggested that the solid-liquid system includes both Helmholtz and Gouy-Chapman layers in a two plate capacitor system. The three models are presented in Figure 2.11. Specific adsorption of ions at the solid surface was added by Graham in 1947. Double layer theory has been used to predict the compressibility behaviour of pure clays (Bolt, 1956; Sridharan and Jayadeva, 1982).

Two groups which worked independently on the stability of colloidal systems (Derjaguin, Landau, Verwey,and Overbeek) reached at the same answers about the forces prevailing in a colloidal solution: the Van der Waals attraction and electrostatic repulsion (Park and Seo, 2011). The DVLO theory, thus, explains the force interaction between two particles of a colloidal solution, with application in many fields.

Another approach -by the field of Molecular Dynamics (MD)- to understand force fields in clay is to calculate the force field of a clay structure in aqueous solutions as a result of the most important atomic interaction forces. This requires a molecular model of clay phases based on experimentally studied minerals (Cygan et al., 2004). Subsequently, using these MD models, more elaborate interactions between clay minerals can be studied (Ebrahimi et al., 2014), and further simplified in interaction potentials for mesoscale particle level simulations (Ebrahimi et al., 2016).

## 2.2 Natural soil mixtures

Natural soils rarely are mono-disperse systems. More commonly they consist of different kinds of particles depending on their geological history. Fine-grained natural soils are dominated by the behaviour or the finest fraction of soil (clay and silt), even though this is not necessarily expressed proportionally by mass ratio of soil constituents, as expressed by various classification methods, *e.g.*, BS 5930 (1999).

However, the constituent fractions indicate whether the anticipated behaviour of soil will be closer to colloidal or frictional material. Muir Wood and Kumar (2000) demonstrated that the mechanical behaviour of heterogeneous soil mixtures of kaolin clay and uniform sand is governed by the response of the clay matrix until the clay fraction drop below 40% by mass. The physical nature of the inter-particle forces that prevail at different particle scales and their interaction lengths, is presented by Santamarina (2003) in Figure 2.12.

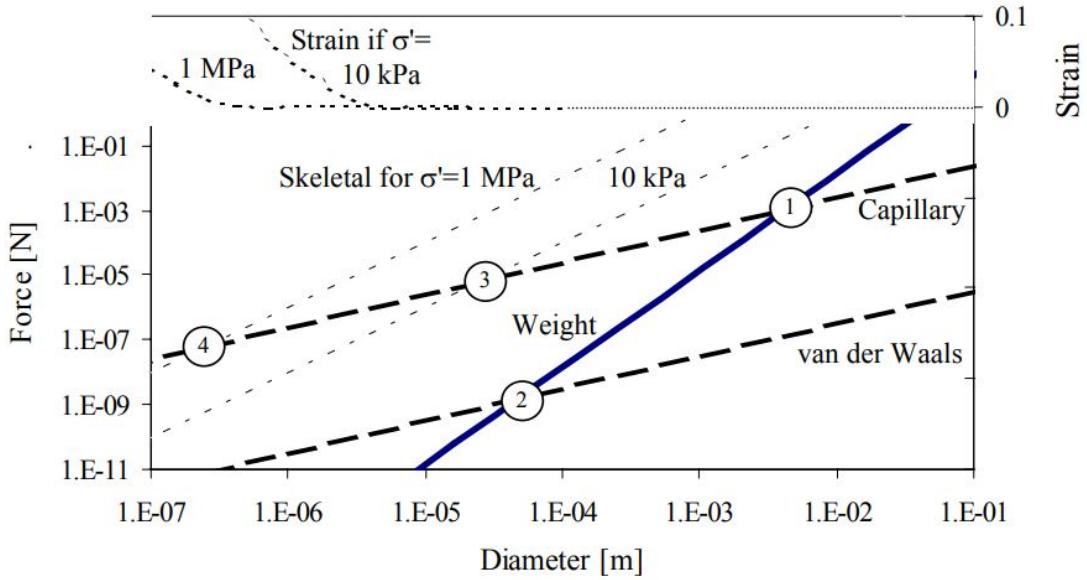


Figure 2.12: Different type of forces (skeletal, capillary, electrical) on soil particles. The upper part of the figure shows the strain (axis on right) caused by changing the pore fluid ionic concentration from fresh-water to seawater conditions (Santamarina, 2003).

## 2.3 Sensitive clays

Soft sensitive clay is a type of a clay soil that, compared to most other soils, is characterised by unfavourable hydro-mechanical properties, such as low strength and stiffness in the normally consolidated range, large void ratio ($e$>2), and a very low hydraulic conductivity. Nevertheless, the undrained strength of intact sensitive clays can by relatively high. Additionally, the inclination of the critical state slope $M$=1.4 for natural water contents around $w_t$=80% suggest a high friction angle under drained conditions. Furthermore, some natural clays have a high sensitivity (ratio of peak undrained shear strength and the remoulded undrained shear strength) in the range of $S_t$=30-300, which might trigger (progressive) failure mechanisms resulting from a modest increase in porewater pressures. The processes leading to failure are characterised by a small magnitudes of strain until peak strength is mobilised, followed by strain-softening that is large in magnitude when compared to other clays. In the case of cyclic loading of sensitive soils, the failure is strongly affected by the strain amplitude, as well as the loading frequency (Wichtmann et al., 2013). Soft

sensitive clays are typically mixtures of fine-grained constituents (silty clays and clays), consisting of a large fraction (>30% by mass) of clay. When the mean particle size ranges between nano- and micro- scale, the electrical forces of charged particles govern the particle arrangement and result in complex colloidal systems. The natural clay tested in this thesis is a medium sensitivity clay ($S_t \approx=$ 30-40) from a test site near Gothenburg in Sweden. Failure in sensitive clay is initiated by a sudden collapse of the initial structure (bonds and fabric), which leads to major softening (loss of strength and stiffness) and a larger viscosity decrease (Khaldoun et al., 2009). The following Subsections will further elaborate some of the important hydro-mechanical mechanisms of sensitive soils as observed at engineering scale.

### 2.3.1 Sensitivity

The sensitivity is defined as the ratio of undrained shear strength of the intact material and the undrained shear strength of the remoulded material (at a constant water content). In Sweden, the sensitivity is typically measured in the laboratory using the fall cone test (Torrance, 1983; EN ISO 17892-6:2017, 2017), though laboratory and field vane tests are also used.

$$S_t = \frac{S_u\ (Undrained\, shear\, strength, intact)}{S_{ur}\ (Undrained\, shear\, strength, remoulded)} \tag{2.1}$$

Sensitivity is linked to thixotropy, i.e., a slow recovery of the microstructure after a forced structural re-alignment under shear (Díaz-Rodríguez and Santamarina, 1999; Mitchell and Soga, 2005; Barnes, 1997; Osterman, 1963). Sensitive clays show a large degree of strain-softening, under mechanical perturbation which can be described by an irreversible phase transition from a dense colloidal gel to a liquid state. Several catastrophic landslides started in highly sensitive clay deposits due to an abrupt loss of strength as a result of a sudden irreversible collapse in microstructure that led to a irreversible phase change, *i.e.* quick clays (Gregersen, 1981; Jakobsson, 1952; Cruden and Varnes, 1996).

The origin of high sensitivity in natural clay deposits is attributed to the colloidal nature of the water-clay system of which the physico-chemical response evolved during slow geological processes that changed the pore water chemistry. Fresh water from melting glaciers and groundwater flow leached the clay, that was originally deposited in a saline environment. Whilst the pore water chemistry, and therefore the physico-chemical equilibrium of the interaction forces, changed over (geological) time, the dense colloid system was mechanically restrained. Different phenomena can result in increase of sensitivity (Osterman, 1963). For the case of marine clays, sensitivity can be caused by leaching of the initially high ionic content by fresh water caused by the isostatic post-glacial uplift and groundwater flow, in particular when exposed to artesian conditions. A high ionic content of the pore water shrinks the Stern layer and attractive forces between the particles prevail. On the contrary, when the ion concentration is reduced, repulsive forces are increased in the new equilibrium. Nevertheless, sensitivity is not only observed in marine clays. Clay deposits in fresh or brackish environments also exhibit sensitivity in many cases.

This is usually linked to the dispersing agents that are released by local sources of organic matter. Rosenqvist (1966) additionally notes the important contribution of coarser grains embedded in fine-grained clays for the emerging sensitivity. A possible explanation for the geological origin of these soil deposits is that during deposition at a fast rate the coarser grains are mixed in within a structure with predominantly finer clay particles. The coarse fraction in these natural sediments contributes to the high peak strength of the undisturbed material that has a large void ratio compared to other natural clays.

Shear thinning is always observed in sensitive clays, however, the subsequent regain in strength due to particle re alignment is not as evident. In the literature, there are contradictory findings about the thixotropic response of clays regarding the extent of their ageing after perturbation. These inconsistencies could be attributed to different factors, such as the different origin of sensitivity for marine and fresh water clays, as well as the different methods to acquire strength measurements in the laboratory or the field. Some highly sensitive quick clays exhibit negligible thixotropy and small strength gain after remoulding (Rosenqvist, 1953). On the contrary, for Scandinavian and Canadian clays ageing effects have also been linked to changes in pore water chemistry (Torrance, 1976) (Lessard and J. Mitchell, 1985). The latter is to be expected, as the physico-chemical environment influences strongly the thixotropic response of the clay matrix (Söderblom, 1966).

### 2.3.2 Rate dependency

Normally and lightly overconsolidated sensitive clays (OCR $< 1.5$) exhibit strong rate dependency, i.e. the magnitude of the emerging stress (deformation) is dependent on the strain (stress) rate applied. At large strain rates, this rate dependency is governed by the hydraulic properties (time scale associated to flow $T_c$ is equal or larger than the time scale for load application $T_l$) that in turn is controlled by the stiffness of the water and the hydraulic conductivity of the clay. This mechanism is readily observed in undrained triaxial tests (Graham et al., 1983; Lefebvre and LeBoeuf, 1987; Zhu and Yin, 2000; Yin et al., 2010). At low loading rates, when $T_c < T_l$, the rate dependency is affected by the clay structure. As opposed to intact natural clays, remoulded natural clays show significantly lower deformation rates (creep) after load application that are independent of the loading magnitude (Li et al., 2018). From strain-rate controlled, Constant Rate of Strain, oedometer tests, it appears that the emerging stiffness and strength and the on-set of yield (apparent preconsolidation pressure) is affected by the strain rate (Sällfors, 1975; Leroueil et al., 1985). Moreover, the rate-dependency at low strain rates is affected by the loading history and stress ratio (deviatoric stress over mean effective stress), which affect the structure and stress state at the start of the creep stage (Tavenas et al., 1978; Fodil et al., 1997; Gao et al., 2020; Zhao et al., 2020). For normally consolidated and lightly overconsolidated sensitive clays that contract, this response is captured well by constitutive models developed for soft soils (Wheeler et al., 2003; Grimstad et al., 2010; Yin et al., 2010; Sivasithamparam et al., 2015).

### 2.3.3 Anisotropy

The emerging hydro-mechanical response, such as the strength, stiffness and hydraulic conductivity of sensitive clays is anisotropic. This is linked to the geometrical anisotropy of the particle arrangement and the resulting anisotropic fabric and pore system. The stress history from deposition to subsequent consolidation under gravity loading, has influenced the particle arrangement from the sedimentation process until the present. In most deposits with sensitive clays, the in-situ stress state is anisotropic, with values for the in-situ coefficient of earth pressure at rest $K_0 = \frac{\sigma'_h}{\sigma'_v} \approx 0.5 - 0.6$ -for Swedish clays (Larsson et al., 2007; Olsson, 2013). Systematic experimental studies into the anisotropic response of sensitive clay, using drained stress probing in triaxial space, show that the anisotropy evolves as function of the stress ratio. Stress ratios that differ significantly from the stress ratio used to create the initial anisotropy in the sample (intact from natural deposit or created during reconstitution) induce a change in anisotropy (as monitored from the ratio of deviatoric and volumetric strains) to a new state (Wheeler et al., 2003; Karstunen and Koskinen, 2008). Considering the typically low hydraulic conductivity of sensitive clays, such experimental programmes are rare.

# Chapter 3

# Multi-scale experiments on natural sensitive clay

## 3.1 Multi-scale monitoring of clay structure

The emerging hydro-mechanical response of sensitive clays at macroscale arises from a complex combination of different mechanisms (physico-chemical and hydro-mechanical) through different scales. In the current work, the material will be investigated using a selection of multiscale observations (Figure 3.1), to arrive at an unbiased investigation of the fabric of the sensitive clay studied at all the relevant scales.

Recent studies (Deirieh, 2016; Deirieh et al., 2018) have demonstrated that the different water replacement techniques, necessary for SEM and MIP, change the resulting geometry of the clay fabric. Therefore, the methods used in this study are restricted to techniques that enable probing of the material in its natural, unaltered, wet state. This eliminates the experimental bias of the method on the structure of the sensitive clay, and additionally offers the potential of real-time continuous measurement of internal structures and their evolution.

The pore networks of natural sensitive clays are usually fully saturated with water, when properly sampled and stored prior to testing. This is not pure water; the additional ionic compounds create an electrolytic solution that affects the behaviour of the natural clay. Both the physico-chemical response at particle scale, and the emerging hydro-mechanical response at engineering scale, of the material that are inter-linked, are affected. The in-situ ionic content evolves over time, depending on the geological and anthropogenic loading history and the groundwater flow, thereby changing the clay properties over time. All tests were performed starting from the initial natural water content of the material in-situ.

In this thesis, the investigation focuses principally on the fabric changes of the sensitive clay. As opposed to methods developed for coarse grained geo-materials (Dijkstra and Broere, 2010; Hall et al., 2018), it is impossible to locally measure the interaction forces between particles (stress) complementary to the fabric changes, in consolidated natural fine-grained soils.

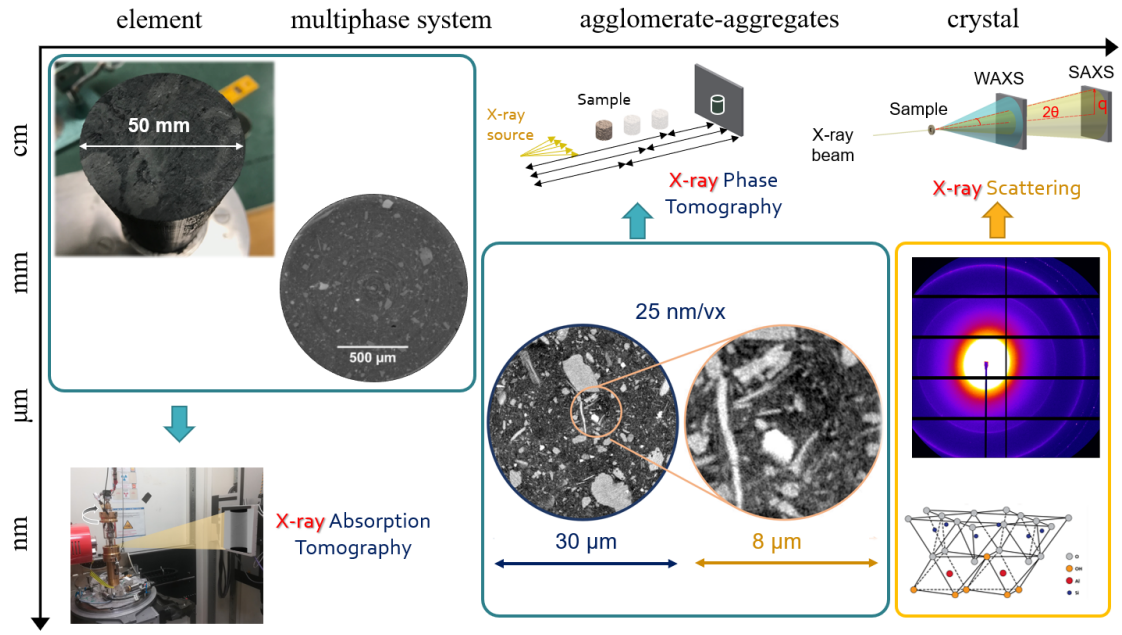


Figure 3.1: An overview of the experimental methods used in this thesis to investigate the changes in the fabric of a natural sensitive clay during hydro-mechanical loading.

### 3.1.1 X-rays

Various non-invasive techniques utilise high energy radiation that penetrates the matter and reacts with it in a non-destructive manner. X-rays are one of them. X-ray radiation has shorter wavelengths (hence higher frequency and higher energy) than visible light, in the range of 0.01 to 10 nm (Figure 3.2).

X-rays react with the matter in different manner: photoelectric absorption, inelastic and elastic scattering, pair production of electrons and photodisintegration (Cartz, 1995). This Section is limited to discussing X-ray - matter interactions that have been used in this work to quantify the evolution of clay fabric and the 3D deformations at meso-scale.

#### Absorption and refraction of X-rays

Many optical processes of X-rays, such as absorption, transmission and refraction (Figure 3.3) are summarised by the complex refractive index:

$$n = 1 - \delta + i\beta \tag{3.1}$$

where $n$ is the index of refraction, $\delta$ is the refractive-index increment and $\beta$ is the absorption index (Rubensson, 2016) and $i$ the imaginary unit.

The wave propagation Equation in vacuum and matter, respectively, is elaborated in Eq. 3.2, Eq. 3.3 & Eq. 3.4.

$$E(x,t) = E_0 e^{i(k_0 x - \omega t)} \tag{3.2}$$

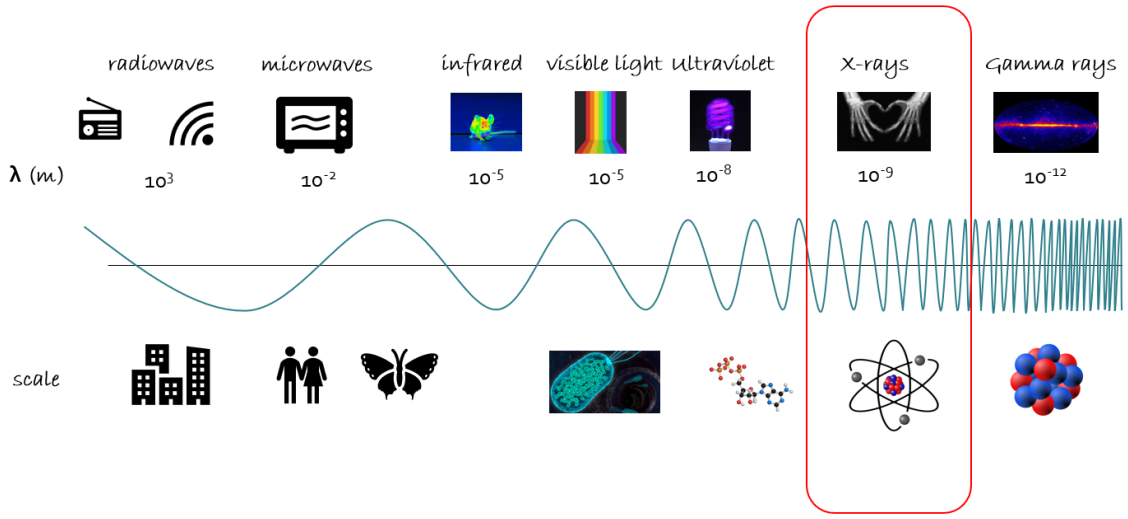


Figure 3.2: Schematic chart of the electromagnetic radiation spectrum.

$$E(x,t) = E_0 e^{i(nk_0x-\omega t)} \tag{3.3}$$

$$E(x,t) = E_0 \underbrace{e^{-\beta k_0 x}}_{exponential\ decay} \underbrace{e^{i[(1-\delta)k_0x-\omega t]}}_{temporal\ term} \tag{3.4}$$

where $E$ is the electric field strength and $E_0$ its amplitude, $x$ is the position in the direction of the wave propagation, $t$ is time, $k_0$ is the wavenumber, $\omega$ is the angular frequency, $e$ is Euler's number.

The measured intensity $I$ is proportional to the electric field squared $E^2$ ($I_0$ and $E_0$ are the respective amplitudes), from Eq. 3.4:

$$I = I_0 e^{-2\beta k_0 x} I = I_0 e^{-\mu x} \tag{3.5}$$

where $\mu$ is the electron density related to the linear attenuation coefficient.

### Coherent Scattering

Coherent X-ray Scattering occurs when X-ray radiation excites electrons to oscillate in the same frequency. This oscillation produces emitted radiation of the same wavelength, *i.e.*, scattered radiation without any energy loss and phase change. The theoretical framework for analysis in X-ray Scattering is based on Bragg's Law:

$$n\lambda = 2dsin\theta \tag{3.6}$$

where $d$ is the distance between atomic layer of a crystal structure, $2\theta$ is the scattering angle, $\lambda$ is the wavelength of the incident X-ray beam and $n$ is an integer.

As can be observed in Figure 3.4, the interference of an incident X-ray with a crystal structure of characteristic $d$ spacing is constructive (producing a wave with the same phase, wavelength and double amplitude) when Bragg's law is satisfied.

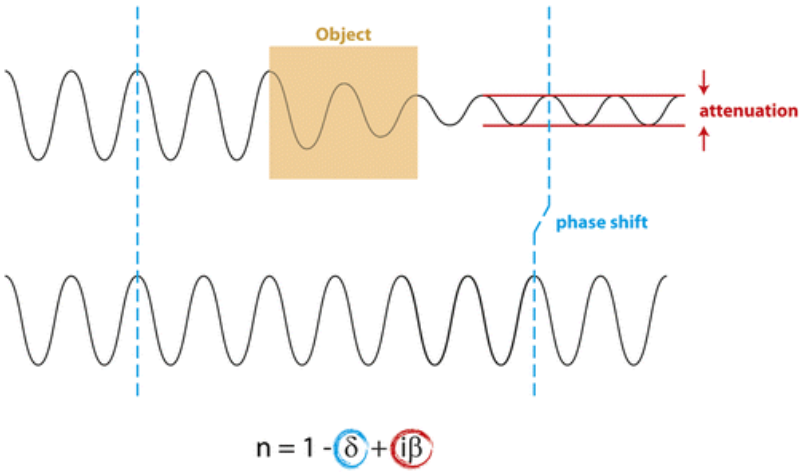


Figure 3.3: Amplitude attenuation and phase shift of an X-ray traversing through an object (Auweter et al., 2014).

In crystallography, the term diffraction is commonly reserved for describing coherent scattering of X-ray with highly ordered materials that have a periodic arrangement of unit cells. This does not limit the use of scattering techniques to investigate materials at larger length scales and thus smaller scattering angles.

X-ray Scattering is a family of non-destructive methods, which utilise the elastic scattering of X-rays to provides bulk measurements of the structure of scatterers in the Å to nm range. Small Angle X-ray Scattering (SAXS) refers to very low scattering angles (0.1°-10°) that can allow capturing of heterogeneities in the submicron range. Wide Angle X-ray Scattering (WAXS) is positioned in between SAXS and diffraction. For even larger spacings, Ultra Small Angle X-ray Scattering (USAXS) should be employed. In scattering analyses, instead of the scattering angle $2\theta$, the scattering vector or momentum transfer $q$ is preferred (Figure 3.5) as described by Eq. 3.7.

$$q = \frac{4\pi}{\lambda} sin\theta \tag{3.7}$$

The radial distance of illuminated pixels from the centre of the transmitted beam on the detector (measured in photon intensity) is the reciprocal of the unit spacing of structures in the sample (Eq. 3.8).

$$q = \frac{2\pi}{d} \tag{3.8}$$

## 3.2 X-ray Scattering

### 3.2.1 Experimental Method

A schematic overview of a typical scattering experiment is shown in Figure 3.5. The X-ray beam incident on the sample is scattered by the sample before hitting the detector. For each point of incidence, the data represents an integrated bulk measurement for a volume that is dictated by the size of the X-ray beam and path

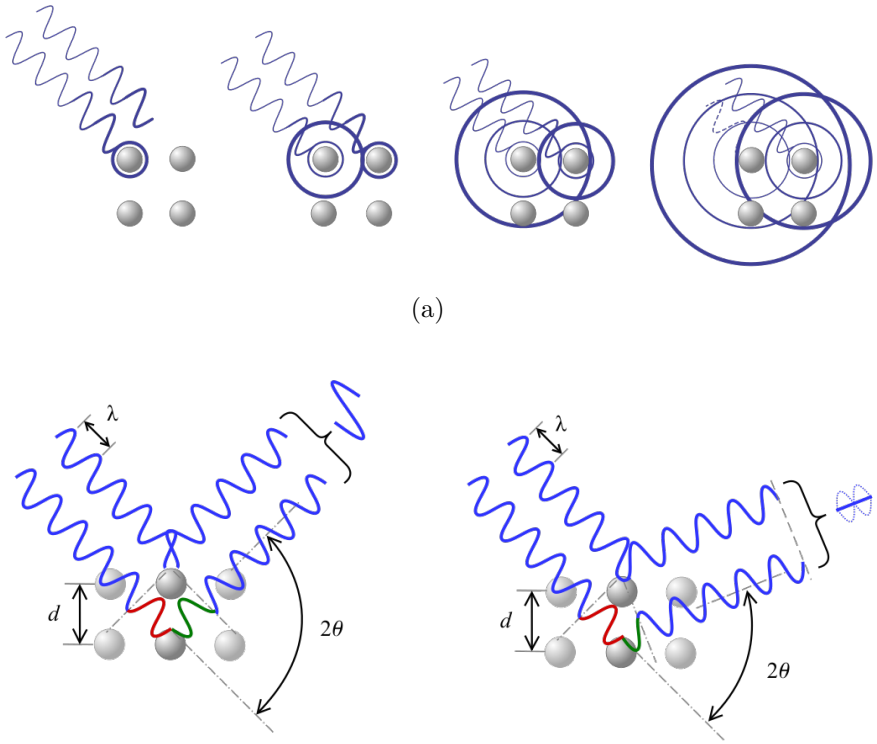


(a)

(b)

Figure 3.4: Bragg's Law schematic representation of constructive and destructive interference. (source: Wikipedia)

length through the sample (approximately the thickness of the sample along the beam). X-rays that are not scattered ($q$ close to 0) are blocked by a beam stop in front of the detector, to improve the signal to noise of subtle scattering events.

The 2D signal is exported from the detector (Figure 3.5) in a form of a 2D array similar to a digital image. Structural information is extracted from the radial sections of the intensity to $q$-range as 1D curves (Figure 3.6). The photon intensity of the detector accounts for the number of the scatterers (electron density) in the illuminated volume. Thus, areas with higher intensities on the X-ray sensitive detector (or respectively the peaks of the 1D SAXS curve) are signs of characteristic repeated spacing in the sample. A great advantage of SAXS compared to traditional direct space microscopy is that it offers the possibility for real-time measurements during different types of probing (mechanical, chemical, etc.).

### 3.2.2 Nanoscale fabric investigation in sensitive clay using SAXS

The physical interpretation of the data relates to the $q$-range configured. At the available range for Wide and Small Angle X-ray Scattering, important information can be obtained for changes at the nm scale (i.e. the intraparticle spacing of clay), as well as for the distribution of this spacing around the azimuth. The latter is

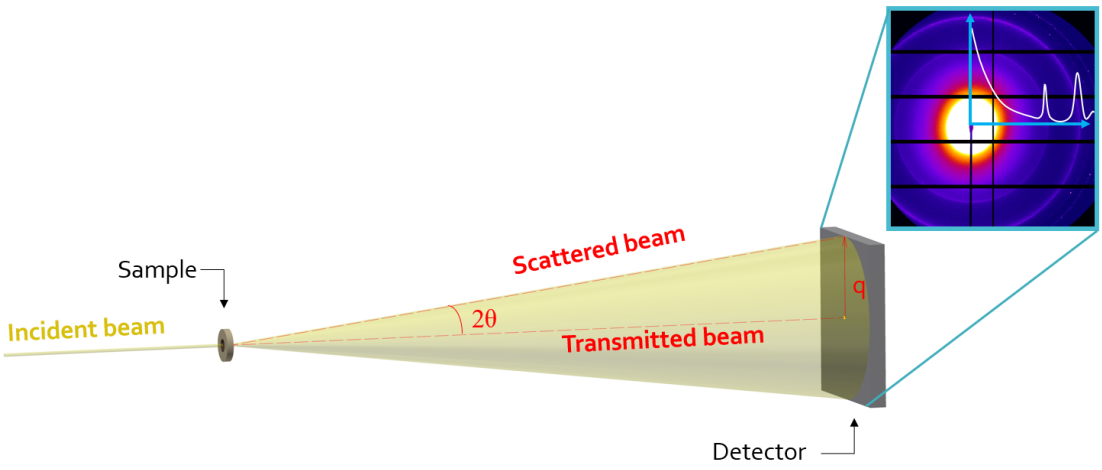


Figure 3.5: Schematic representation of a small-angle scattering experiment. The incident and scattered beams are shown, along with the resultant scattering vector $q$, which is in the plane of the detector. The analysis is based on the distribution of photons as function of $q$.

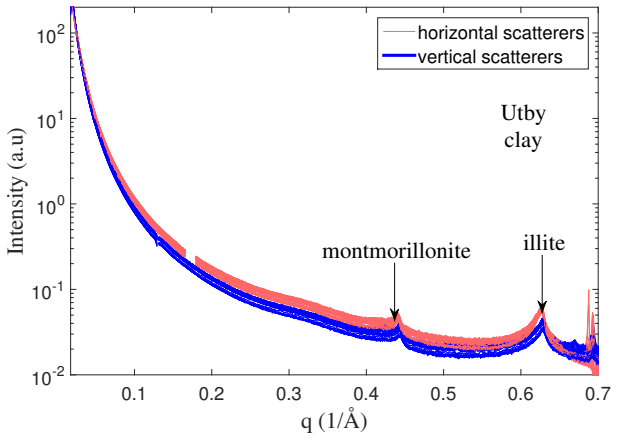


Figure 3.6: SAXS 1D curve of $q$-range *vs.* intensity. Peaks indicate characteristic spacing. This 1D curve refers on a clay sample with two mineral composition.

an indirect measure of particle orientations. A wide range of scattering angles was investigated, from WAXS to SAXS to trace the most effective $q$-range to yield information on the clay investigated (Paper I).

The first observation on the SAXS signal is the identification of the peaks that correspond to a mineral (Figure 3.6). Moreover, the intensity of the peak for different azimuth angles can give the orientational distribution to the horizontal. Although there are additional mechanisms that can reduce the intensity of the incident X-ray beam as it passes the sample, even changing the wavelength of the produced X-ray (Cartz, 1995), in this work the focus is on the change in intensity distribution from major scattering events.

The successful use of scattering measurements is demonstrated for the case of a kaolin slurry consolidated at high vertical stress (Figure 3.7), i.e. Paper II. It is expected that in the slurry the particles are randomly dispersed (due to

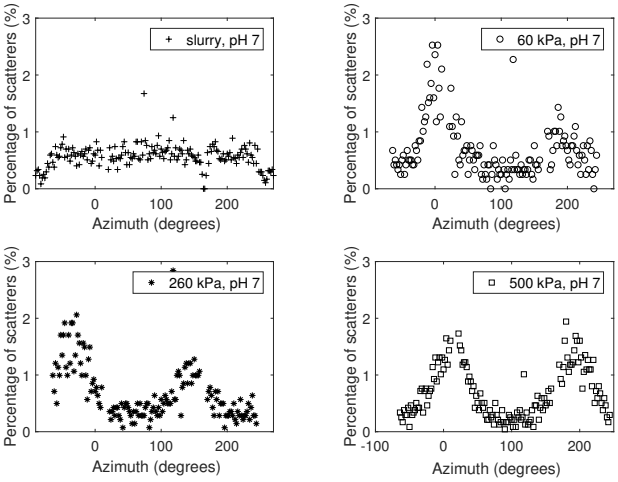


Figure 3.7: Scattering orientation through the azimuth for kaolin slurry and the subsequent consolidated samples at vertical effective stress levels of of 60 kPa, 260 kPa & 500 kPa.

mechanical stirring) and are gradually aligned closer to the horizontal plane during axial consolidation.

A great challenge for natural clay samples is to conduct the scattering experiments on an undisturbed intact specimen extracted from the field (not reconstituted in the laboratory). The natural clay that is investigated consistently throughout this research project is a natural clay of medium sensitivity from the Utby test site, Gothenburg, in Sweden.

A specially designed set-up for a real-time SAXS measurement during 1D compression was designed (Paper III). A thin-walled glass capillary was cut into a natural clay sample, to contain it and used as the compression cell (Figure 3.8). The scattering signal of an empty capillary was used to correct the data in subsequent analyses. The sample had to be very thin (1 mm thickness) to minimise attenuation and to obtain a scattering signal with adequate signal to noise level at moderate acquisition times (minutes). Simultaneously, a continuum description of surface deformations was obtained by tracking the natural speckle of the specimen using a stereoscopic camera system and subsequent 2D surface DIC. The stress-strain response at continuum scale was correlated to the evolution of the intra-particle spacing and the particle orientation.

The change of intra-particle spacing was observed only for one of the two minerals (illite and montmorillonite) in the clay, the expandable one (montmorillonite). The change is evident only after the monotonic compression has finished (Figure 3.9). The emergence of a new peak was further validated in extensively mechanically remoulded clay samples. Cyclic loading of the miniature specimens also exhibited the appearance of the new peak only after the end of the cycles.

Additionally, the orientational distribution of the two minerals was examined. Although, both minerals (illite and montmorillonite) followed a common trend by aligning closer to the horizontal plane during compression, their absolute orientation was dissimilar. This interesting observation requires further study with techniques

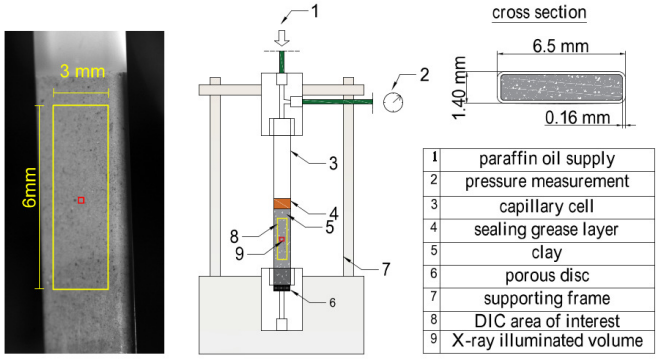


Figure 3.8: A capillary 1D compression cell (middle) contains the clay specimen in its natural water content, whilst simultaneously enabling surface DIC measurements (left) and X-ray transmission through it (cross section on the right).

that can resolve the 3D structure, in order to understand the spatial configuration of both minerals.

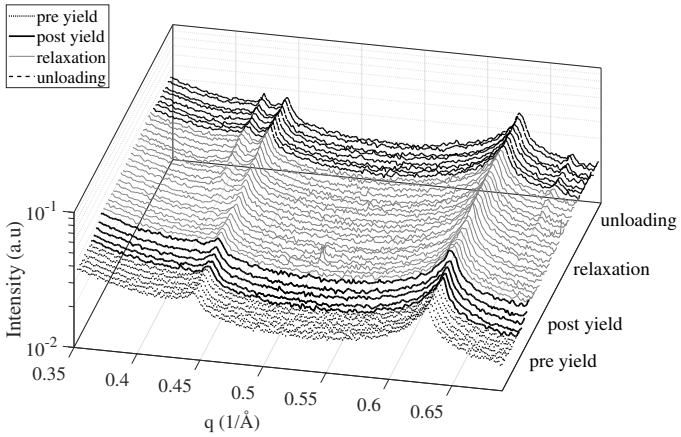


Figure 3.9: A new peak is emerging for the montmorillonite mineral after monotonic compression.

## 3.3 Phase contrast tomography

Regardless of the great capabilities that it offers for a wide range of materials, X-ray absorption tomography typically is restricted to µm-range spatial resolution. In contrast, phase tomography, due to its edge enhancement capabilities, can provide an improved spatial resolution down to the nanometric range (Paganin et al., 2002), as can be shown for the sensitive clay tested in Figure 3.10. In this approach, we try to span observations of clay structure from nano- to millimetre scale, from intraparticle level to continuum scale. Clay particles, however, are often nanoscale structures, which pushes the limits for the attainable spatial resolution for X-ray Phase Tomography for the natural clay samples tested at the ID16B (nanotomography) and ID19 (microtomography) beamlines in ESRF, Grenoble, France.

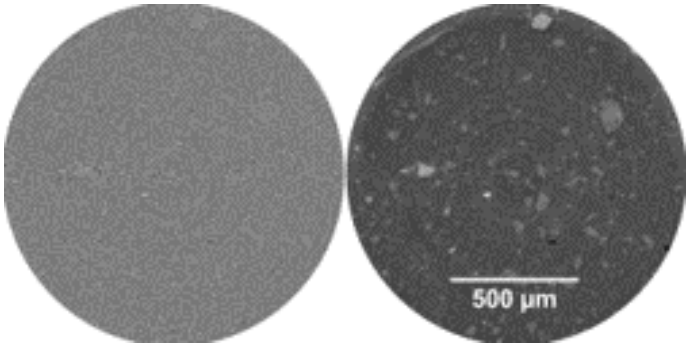


Figure 3.10: Tomographic sections of sensitive clay specimens (Utby clay), using absorption (left) and phase (right) contrast techniques.

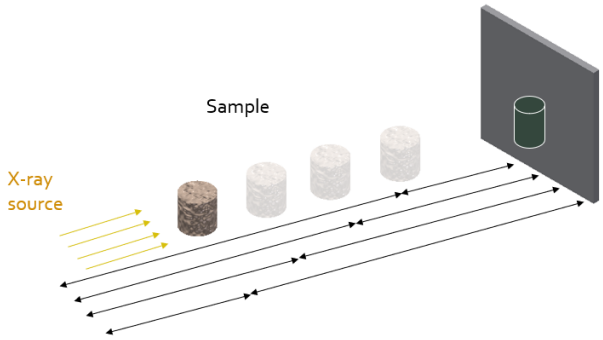


Figure 3.11: Schematic representation of quantitative phase tomography.

ID19 is microtomography beamline at the synchrotron, that offers XCT with absorption and phase contrast. A great advantage of synchroton radiation is the high brilliance of the the X-rays and the spatial and temporal coherence (Weber, 2016). Phase contrast can be retrieved by various experimental and numerical methods. At ID19, a numerical phase contrast retrieval method (Paganin et al., 2002) was used. Different magnification values provided the 3D images of a 10 mm natural (Utby) clay sample as presented in horizontal slices in Figure 3.12a, 3.12b, 3.12c.

ID16B is a hard X-ray beamnline (with energy levels $> 10$ keV) dedicated to nanoscale imaging of microscopic samples. Glass capillaries of 300 $\mu$m diameter, sealed on both sides by grease paste, were used to contain the clay sample at constant water content. The phase contrast was computed from a series of absorption tomographies at different sample-detector distances (Cloetens et al., 1999), as presented in Figure 3.11. Four different images were acquired to construct the final phase contrast tomography. The resulting voxel size was 25 nm and the Field of View (FoV) was 64x54 µm. This field and the real resolution resulting from the contrast and the voxel size should be sufficient to discern inter-particle clay fabric. Figure 3.12d shows an horizontal slice from the nanotomography performed at the natural clay sample. This is the first time a wet unaltered state of natural clay is captured in 3D with nanoscale spatial resolution.

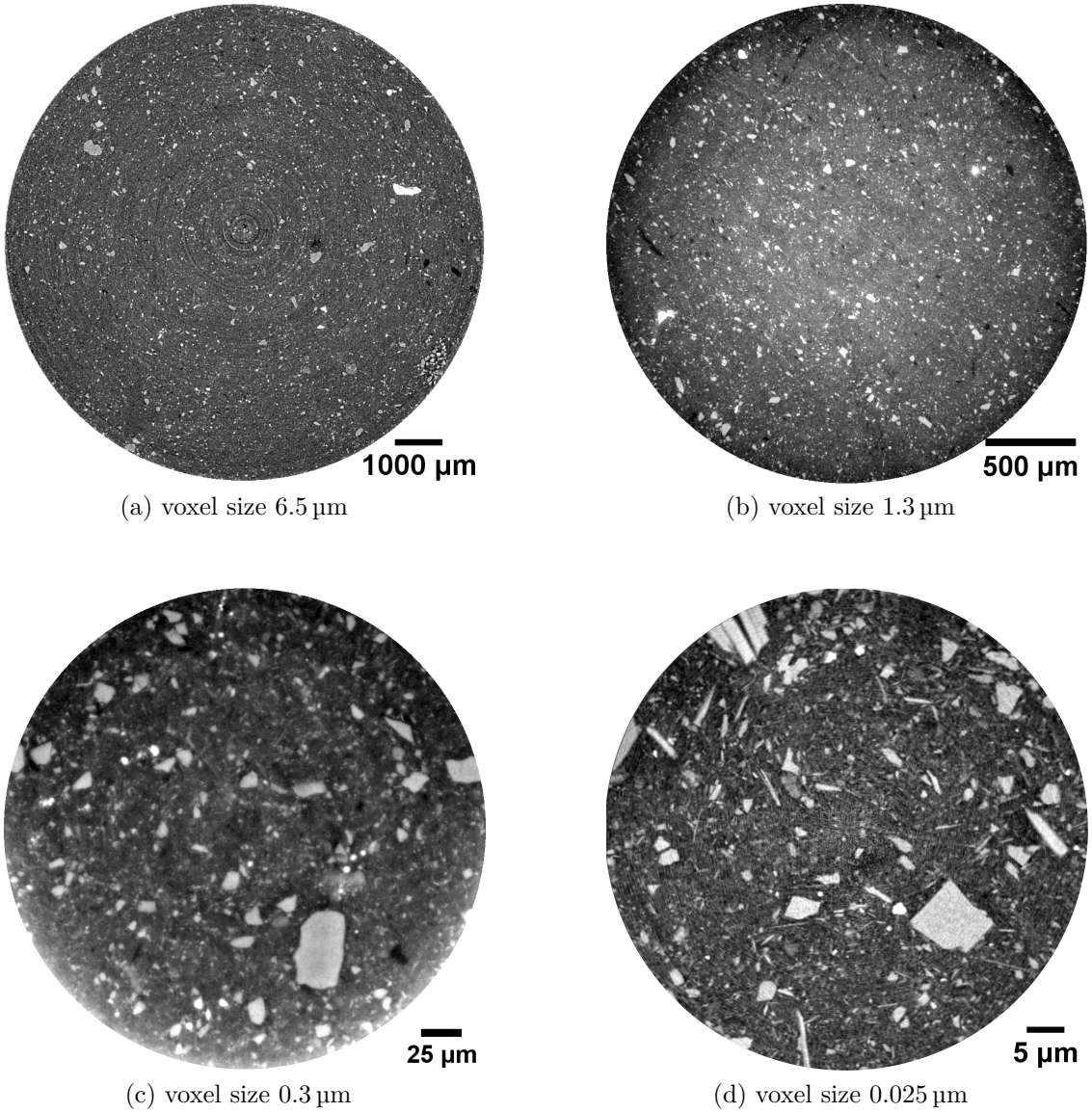


(a) voxel size 6.5 µm

(b) voxel size 1.3 µm

(c) voxel size 0.3 µm

(d) voxel size 0.025 µm

Figure 3.12: Phase contrast tomographies of sensitive clay samples from Utby at different magnification levels.

The presence of silt grains in a wide particle size range is observed even at sub-µm scale Figure 3.12. The smaller clay fractions are still not distinguishable, even at this spatial scale (the dark grey bands in the image). Moreover, there is a large fraction of elongated particles in Figure 3.12d, which consist of a different mineral from the finer clay matrix. A segmented reconstruction, with ImageJ2 software by Rueden et al. (2017), of the elongated particles is presented in Figure 3.13. It is hypothesised that the granular component and larger particles observed in this natural clay sample strongly affects the emerging strength and stiffness response, especially having in mind the differences in the orientational evolution of the two minerals (Paper III). The unique experimental data on the 3D structure supports the importance of non-clay particles in the emerging behaviour of sensitive soils (Cabrera

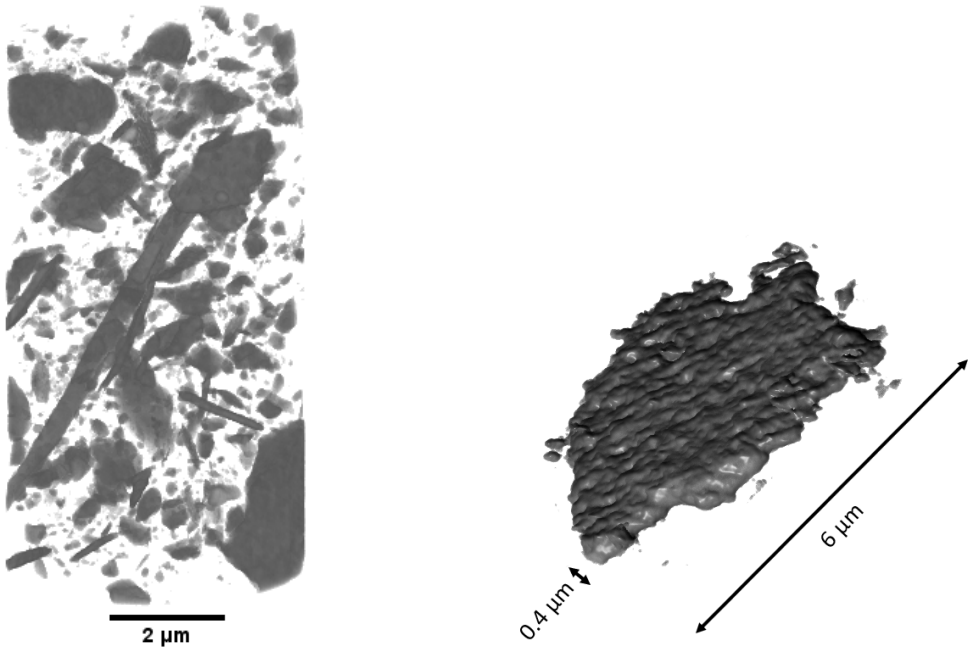


(a) (b)

Figure 3.13: 3D reconstruction of the segmented structure of the near-µm particles (rock flour) on the left and an isolated particle on the right.

and Smalley, 1973).

## 3.4 XCLAY triaxial apparatus

X-ray tomography is a very promising technique for monitoring the evolving internal deformation of soil samples during hydro-mechanical testing. Great advances have been made for testing coarse grained geo-materials with simultaneous monitoring of the internal mechanisms using XCT (Lenoir et al., 2007; Alshibli and Hasan, 2008; Matsushima et al., 2010; Hall et al., 2010; Andò et al., 2012). XCT required scaling the size of the triaxial cell and sample size, but also consideration of the need for cabling and tubing that facilitate 180° or 360° rotation of the sample during a tomographic scan. In the cases above, the triaxial apparatus was designed for simple loading paths such as axial compression, and in a special case extension, at large stress levels (Andò et al., 2017). Furthermore, to reduce complexity, often the cell pressure was not regulated during a scan.

The devices above are inadequate for testing soft clays that require low stress levels, and special attention for sample preparation. In addition, the more advanced drained loading paths required for systematic probing of the constitutive response of clays (see Karstunen and Koskinen, 2008), necessitates continuous control of all pressures during the test.

One of the main motivations for the miniaturisation of specimen size is the favourable scaling of the time duration of the test. By reducing the drainage length by a 1/5, the consolidation time is reduced quadratically, i.e. $1/5^2$ (Muir Wood, 2004). This makes drained testing much faster, something absolutely demanded for tomography at synchrotron beamlines with limited instrument time. In parallel, it facilitates for more meticulous drained stress probing of soft clays.

A bespoke miniature triaxial apparatus has been developed for advanced stress path probing of soft sensitive clays with simultaneous monitoring using XCT. Among the main objectives were the operational versatility, such as compatibility with different imaging facilities and sample preparation, and robust stress control at (very) low effective stress levels $< 5\,\mathrm{kPa}$.

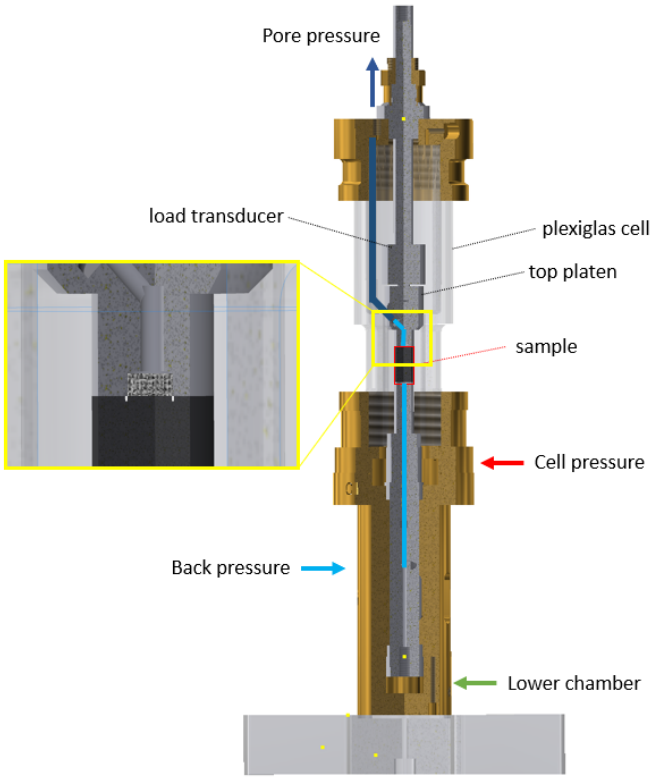


Figure 3.14: Three quarter section view of the XCLAY miniature triaxial apparatus.

The XCLAY triaxial apparatus (Figure 3.14) is a miniature version of a Bishop-Wesley cell (Bishop and Wesley, 1975) with modifications that facilitate advanced testing of natural soft clay samples. The control of the stresses on the boundary of the clay sample is performed by a high precision syringe pump system (neMESYS Mid Pressure Syringe Pumps sourced from Cetoni GmbH 3.1). High precision is necessary when handling so small volumes (sample volume $\approx 1500\ \mathrm{mm}^3$) and low stresses (stress increments 10 Pa).

A limitation of the stress control is the accuracy of the measurement of load and axial displacement, rather than the syringe pump itself. The syringe pumps were used to regulate the lower chamber pressure (for application of axial load), cell

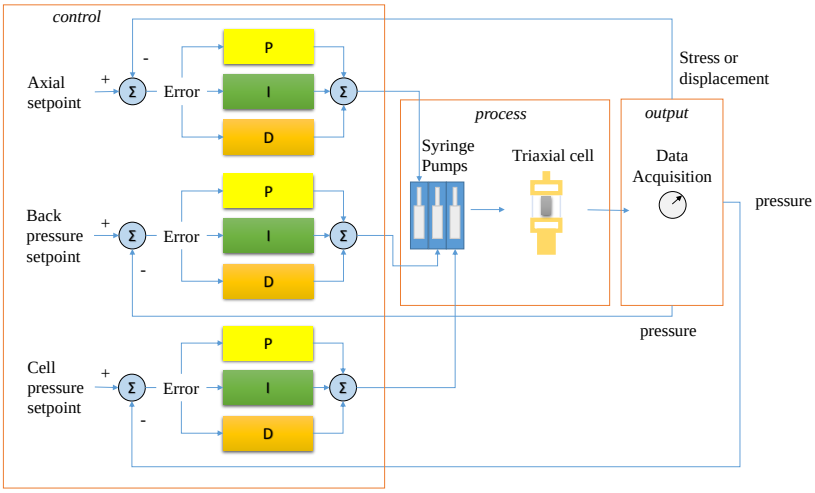


Figure 3.15: Flow chart of the control system for the miniature triaxial apparatus.

pressure (surrounding the sample) and back pressure (pore pressures in the sample). The syringes in this system are modular, which allows to optimise the control volume for the required application, as back pressure control requires smaller volume changes at higher resolution than the control of the cell pressure.

Table 3.1: Performance characteristics of neMESYS Mid Pressure Syringe Pump.

| Module characteristics | |
|---|---|
| max. Plunger Rate | $6\,\mathrm{mm\,s^{-1}}$ |
| min. Plunger Rate. | $1\,\mathrm{nm\,s^{-1}}$ |
| min. Plunger Travel | 3.7 nm |
| max. Linear Force | 1000 N |

Cetoni pumps are computer controlled over USB using the Qmix Software Development Kit (SDK) provided by *Cetoni*, whereas the sensor readings of the axial displacement transducer (LORD MG-LVDT) and pressure sensors (thin-film type pressure transducers) are acquired using a *National Instruments* system (National Instruments cDAQ-9172 Legacy Compact DAQ Chassis with National Instruments NI 9219 24-Bit C-Series Universal Analog Input). The system is controlled using *LabVIEW* (Bitter et al., 2006) as presented schematically in Figure 3.15.

The input of the syringe pumps are set points for the final displacement and the displacement rate of the syringe piston. Through a Proportional–Integral–Derivative (PID) error control loop, the user can define the desired stress path applied to the sample during consolidation, and the subsequent shearing stage. In order to apply radial stress paths in the $p' - q$ space (mean effective stress *vs.* deviator stress) in the temporal range required by the test, a PD control proved to be more suitable, for stress changes typically slow (<1 kPa/min). In a PD system, The Proportional (P) control is the action which restores the error amplitude and the Derivative (D) control is the action keeping the system in balance avoiding large oscillations. Strain-rate

control is also implemented. The capability of nanometre displacement increments of the syringe pumps (Table 3.1) makes the error correction control of the system extremely flexible and adaptable to the desired stress path control. Since the control system is based an a correction feedback loop, the accuracy of the load and pressure sensors limits the system control to 0.25 kPa.

Due to the small size and the low stiffness of the specimens, a special sample mounting procedure is developed. The sample is mounted on the pedestal without being touched by hand to reduce disturbance according to the procedure, as described in Paper IV. Furthermore, a membraneless procedure is adopted. Rather than using a membrane to separate the cell and back pressure applied to the sample a viscous oil (paraffin oil) is used as a cell liquid. Due to its viscosity, the oil cannot penetrate the fine pore system of clay. Obviously, this approach limits the use of the device to soils with a low permeability. The last connection that needs to be sealed is the boundary between the clay sample and the end platens located at the bottom and at the top of the specimen. This is realised by a very thin and short cutting ring, surrounding the porous disc, that penetrated the sample and prevents a direct path between the cell liquid and the pore and back pressure lines at the sample ends (magnified part of Figure 3.14).

## 3.5 Monitoring 4D internal deformations

X-ray Computed Tomography is combined with DVC to quantify the 4D kinematics (three spatial dimensions plus time) in the sample during the stress probing of sensitive clays using XCLAY. A short introduction for these methods, with a focus on their application for geomechanical testing, will be given below.

### 3.5.1 X-ray Computed Tomography (XCT)

XCT enables the study of the composition and internal structure of bulk objects using X-ray radiation. This method provides 3D images of the object scanned with X-rays, based on the measurement of emitted, transmitted or reflected radiation using a reconstruction algorithm. The most common X-ray tomography method is based on the measurement of the attenuation (decrease in energy) of X-rays. This absorption-based tomography, hence, is a logical extension of projectional radiography.

Radiography is the result of transmitted X–ray radiation captured by an X-ray sensitive detector (basically a scintillator that converts X-rays to visible light coupled to a Charged-Coupled Device (CCD) detector). A radiography is an integration of the attenuation path through the sample and cannot resolve attenuation differences along the path (depth). Radiographies at incremental projection angles are acquired to obtain 3D information. Once a necessary number of projections is obtained, the 3D image of the object can be reconstructed from the projections using a filtered back projection algorithm (Feldkamp et al., 1984), as is schematically illustrated in Figure 3.16. The number of projections is a function of the desired resolution, hence the number of points in Fourier space required for the algorithm.

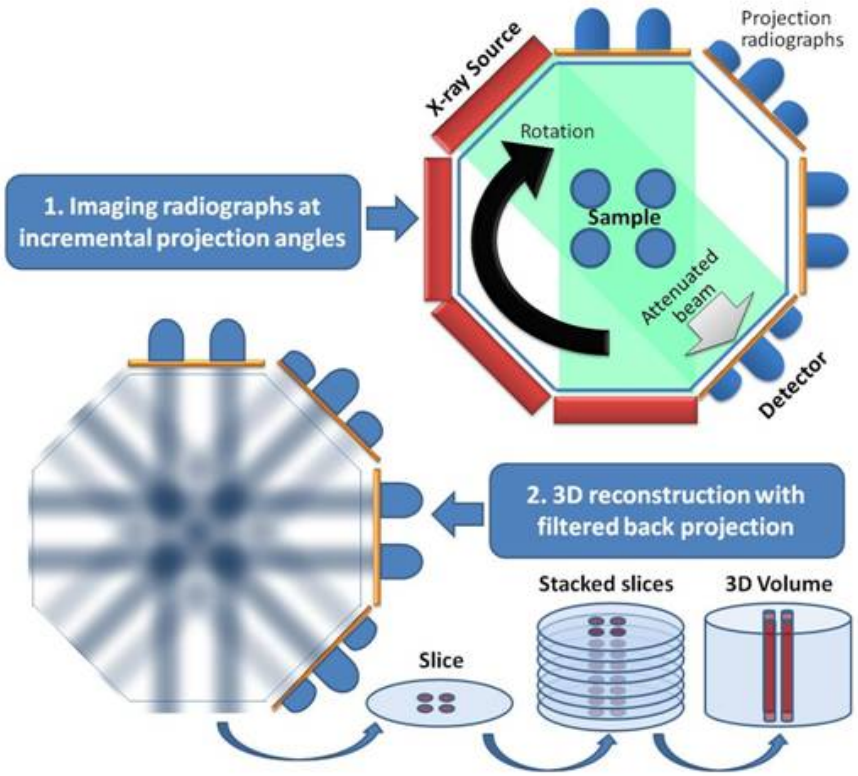


Figure 3.16: Schematic representation of the process generating 3D X–ray absorption-based images from the reconstruction of 2D projection radiographies around the sample. (source: Carnegie Mellon University)

The use of XCT has been an important tool in medical imaging since the 1970s. It has also advanced significantly the study of internal structure of geomaterials during in-situ loading (Hall et al., 2010; Takano et al., 2015; Lenoir et al., 2007). This requires samples with sufficient density contrast, which is a function of the atomic number of the constituents of the sample, at the spatial scale that can be resolved by the XCT setup. For the case of fine-grained soils, such as saturated clays, the natural contrast is only available between the colloidal (clay) and the granular (silt, sand) fractions. Water saturated pores and clay do not have a strong attenuation contrast. Phase tomography techniques offer alternative contrast mechanisms for the visualisation of smaller structures and materials with poor density contrast. In-line or propagation-based phase imaging is used as it is most compatible with the X-ray tomography set ups used for absorption tomography without excessive technical modifications.

In propagation-based phase imaging, X-rays transmitted through the sample at various angles will propagate between the object and the detector via a different path length, hence introducing a wavefront with phase differences. The spatially non-uniform X-ray attenuation and refractive index within the sample contribute to a change in the shape of the X-ray wavefront that passes through the sample (Figure 3.17). A conventional absorption image is obtained, when the detector is located directly behind the sample. In contrast, at larger distances from the object, a

phase-contrast image will be acquired. Interfaces between constituents with differing X-ray refractive indices are enhanced in the final image. Phase-contrast provides a variable enhancement of the conventional attenuation image, because there is also a change of X-ray attenuation across these interfaces (Zhou and Brahme, 2008).

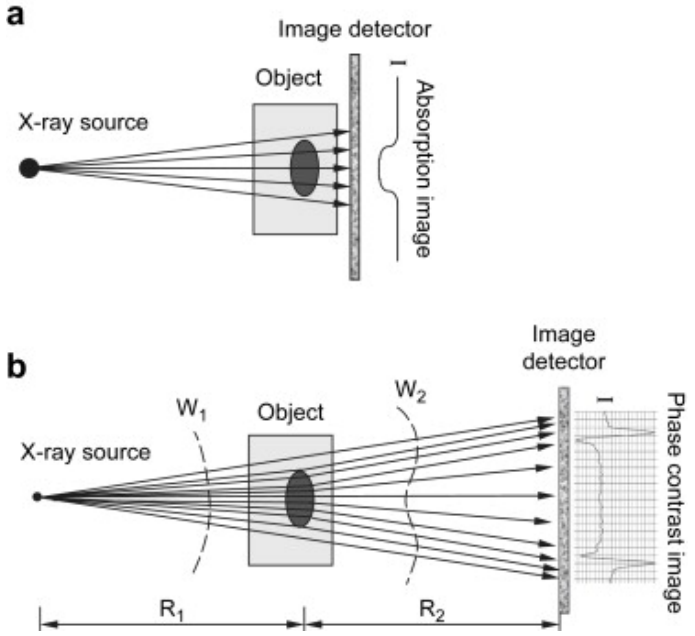


Figure 3.17: Schemes of (a) an attenuation-based imaging configuration and (b) an in-line phase-contrast imaging configuration (Zhou and Brahme, 2008).

### 3.5.2 Digital Volume Correlation

Displacement and strain measurements in traditional experimental mechanics are calculated at element level from displacement measurements at the boundaries of the sample. The analysis of those results assumes homogeneous behaviour of the material within the gauge length of the sensor (Beckwith et al., 2009). DIC offers full-field displacement and strain measurements, which can be particularly useful to reveal the spatially heterogeneous deformations of composite materials, such as geomaterials. The principle of DIC is based on the mathematical comparison of a pair of digital images acquired at different instances of the experiment and relies on features in the image that can be correlated. DIC has become an important field in imaging based metrology both in solid mechanics and fluid mechanics (Sutton et al., 2009; Adrian et al., 2011; Grédiac and Hild, 2012). These 2D or 3D image pairs can be acquired by any kind of imaging technique of processes (*e.g.*, digital photography, X-ray or neutron radiographies). The method requires sufficient spatial intensity contrast in the images, either originating from the physical (surface) properties of the sample, or from tracers that are artificially mixed/seeded/applied to the sample.

Depending on the available data, different types of DIC can be performed, *e.g.*, (Tudisco et al., 2015):

- 2D-DIC: applied on 2D images (*e.g.*, obtained from surface snapshots or X–ray radiographies) applicable to cases of plane-strain tests
- 3D-surface DIC (stereo-vision plus stereo-correlation): demands the acquisition of pair of photos (reference and deformed) from a two-camera system and yields a 3D field displacement vector on the surface of plane stress samples
- 3D-volumetric DIC (or , DVC): requires two 3D images (tomographies) and provides a 3D field of three components of the displacement vector.

In the current research, both 3D surface DIC on digital images and DVC on X-ray tomographies have been employed (Papers III, IV), where the first image is taken as the reference image for the comparison with subsequent images acquired sequentially in time during hydro-mechanical loading. Hence, each image pair represents a new state of deformation. Typically, both images are subdivided in subsets that are subsequently correlated, as such resolving a 2D or 3D displacement field for each state of deformation. Here, two different image correlation approaches have been employed, *i.e.*, image registration and cross-correlation.

Image registration is the process of aligning two images of the same object/scene. A geometrical transformation is applied to the image of the deformed object until it is aligned with the reference image. Basically the problem can be rewritten as a minimisation problem of the error between the reference and the deformed state (Grédiac and Hild, 2012). The parameters of the successful transformation matrix are subsequently used to derive the displacements to obtain the deformed image. Usually a convergence algorithm is applied in the process to accelerate this, and end the process for a minimum error satisfied criterion (Grédiac and Hild, 2012). The robustness of the method allows the method to be used on the full image, *e.g.*, to

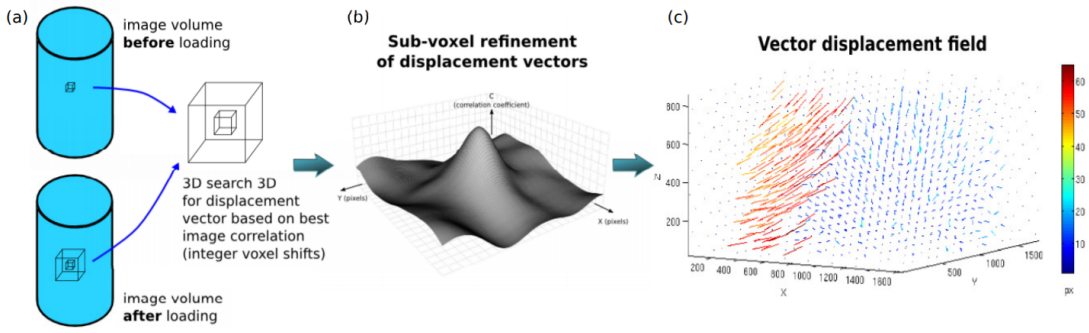


Figure 3.18: Schematics of a 3D-volumetric DIC analysis approach: (a) two subsets of voxels are correlated, moving one of them inside a search window, to find the integer displacement; (b) the subvoxel displacement is given by the maximum of a mathematical function interpolating a set of correlation coefficients; (c) repeating this procedure in a grid of points gives the 3D displacement field (Tudisco et al., 2015).

create a predictor for the displacements, or at subset level, to obtain a displacement field.

Cross correlation is a more conventional approach for the quantification of deformations between an image pair. Cross correlation is calculated from a sliding dot product of subsets of the two correlated images. The maximum of the correlation product (often normalised) represents the new position of the subset in the second (deformed) image. This distance between the original and the new position denotes the displacement of this subset. A full field 2D or 3D displacement field is obtained by repeating this operation for each subset. Figure 3.18 shows a schematic representation of the cross correlation procedure for DVC. The position of the maximum can be refined to sub pixel accuracy by interpolating a continuous function through the map of correlation results.

When properly implemented both algorithms yield subpixel displacement accuracy down to 1/10 of the pixel size. The displacement field calculated from the image data, is subsequently used to calculate the full field strain map.

It should be noted that the size of the subset is dictated by the amount of contrast in the images, which is affected by the sample and the imaging method. As a result, the spatial resolution of the displacement data is two orders lower than the magnitude of the detected displacements.

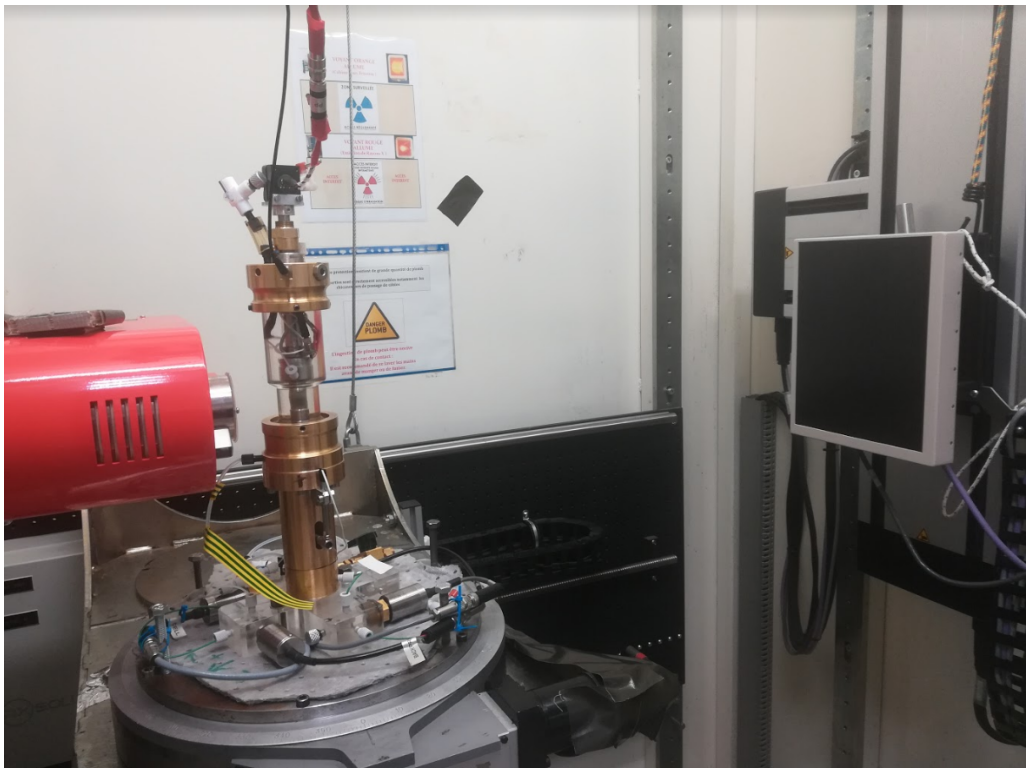

Figure 3.19: XCLAY cell on the rotation stage of 3SR tomograph.

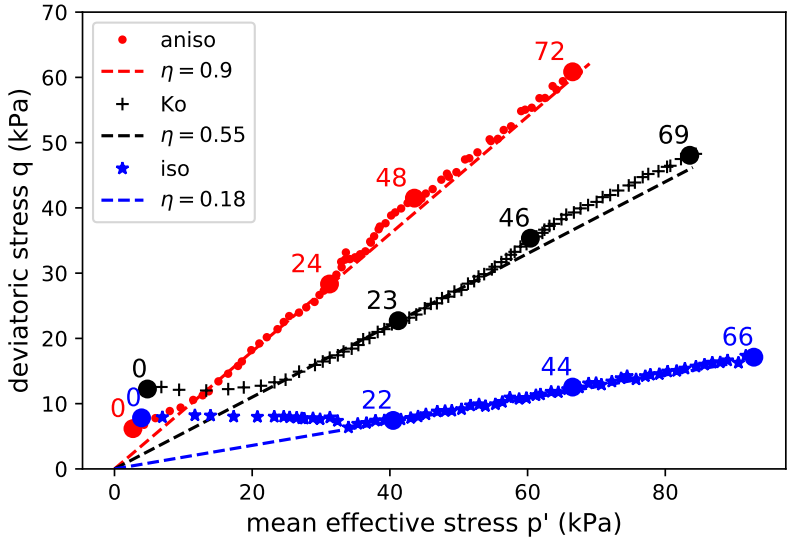


Figure 3.20: Stress paths at various stress ratios.

## 3.6 Mesoscale deformation of sensitive clay in drained triaxial compression

Paper IV presents the results of the study of internal deformations for three different stress paths. The XCLAY triaxial cell was used at the facilities of Labotoire 3SR, in Grenoble, France, to obtain 3D images of miniature (10 mm diameter, 18 mm height) samples of Utby clay (Figure 3.19). The SPAM -Software for Practical Analysis of Materials- (Andò et al., 2017–) Python toolbox was used to extract the 3D full field displacement and strain maps from the tomography data.

In this test series, fabric anisotropy was investigated at mesoscale (µm to mm), using the natural speckle arising from the absorption contrast between the silt grains and the clay matrix. Three drained triaxial tests in compression at stress ratios $\eta$=0.90, $\eta$=0.55 and $\eta$=0.18 were conducted (Figure 3.20).

The focus of the tests in the laboratory tomograph was to obtain data from drained stress probes at a high temporal resolution (time interval of 41 min with an acquisition duration of 20 min). This results in a total number of approximately 70 scans each with 640 projections (728 x 920 pixels) resulting in ca. 500 MB of image data per scan. Considering this large amount of data, the efficient implementation of image registration coupled to cross correlation offered in SPAM proved advantageous for the analysis.

The deviatoric and volumetric strain fields are obtained for every load step as well, as a statistic analysis on the mean values of strain were conducted. Figure 3.21 presents an example of the processed results by plotting the ratio of the deviatoric to mean effective stress ratio ($\eta = \frac{q}{p'}$) and deviatoric to volumetric incremental strain ratio ($\frac{\varepsilon_d}{\varepsilon_v}$) as function of time. Basically, the strain ratio represents the ratio of the second and first invariant of the locally measured strain tensor. The $K_0$ stress path

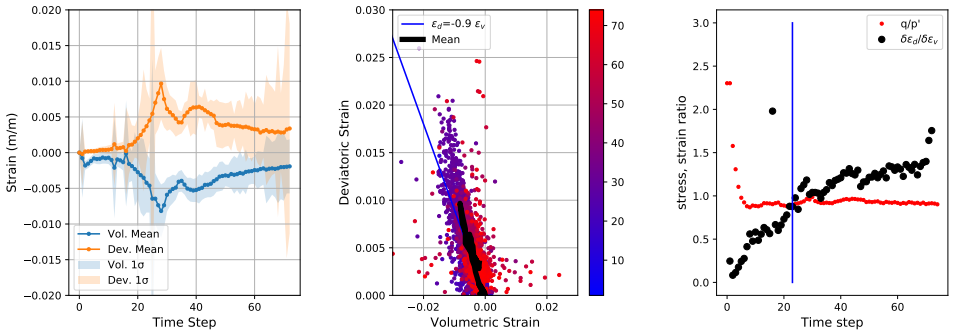


Figure 3.21: Stress and strain ratios for a drained triaxial test on Utby clay for a highly deviatoric stress path with $\eta$=0.90. On the right subplot, the blue line signifies the onset of yield as determined from the stress-strain plot.

resulted in the most homogeneous full-field strain maps, while the highly deviatoric path resulted in very inhomogeneous strain fields. The data is further reduced by plotting the arithmetic mean of all the grid points of the full field strain maps. One of the main findings, fully reported in Paper IV, was that the mean values of this heterogeneous strain field agree well with the global values of strain obtained by the external measurements, and the contour of the sample volume in the tomography data. Furthermore, the boundary value level stress measurements combined with the mean response of the local strain data provides unique data on the relation between the stress ratio and the incremental strain direction (akin to the flow rule, but now with increments of total strain, rather than irrecoverable (visco-plastic) strain).

# Chapter 4

# Conclusions & Recommendations

## 4.1 Conclusions

The aim of the thesis was to quantify the response of natural sensitive clays, spanning from intraparticle to continuum scale, under hydro-mechanical loading. This enables to link the evolving internal material behaviour to the constitutive response at boundary value level. Bespoke miniature apparatuses were developed to facilitate *in-operando* geomechanical testing, *i.e.*, a plane strain oedometer for X-ray scattering experiments and a miniature triaxial cell for monitoring internal deformations of fine-grained soils during hydro-mechanical probing using XCT. A combination of laboratory and synchrotron based scattering and imaging instruments were used successfully for *in-operando* quantification of the evolving fabric in clay across several length scales (nm–mm).

Most of the experiments focused on investigating the fabric evolution in a natural clay with medium sensitivity ($S_t = 30$) from Utby, Gothenburg. The combination of experimental techniques enabled investigation of fabric changes during hydro-mechanical loading through the scales. A major challenge, for obtaining time-invariant snapshots of the evolving material response, was balancing the loading and acquisition rates within the limits of the techniques available with the time-dependent response of the clay tested.

X-ray Scattering provided insight on the nanometre scale (between 0.7 nm to 20 nm), in terms of the integrated response of intraparticle strain and particle orientation. The complexity of the scattering signals for these consolidated non-ordered poly-disperse materials and $q$-range did not permit fitting form factors for the clay particles. In particular, a system of two clay minerals was monitored during a 1D compression test of the sensitive clay. The two minerals identified, illite and montmorillonite experience dissimilar changes during hydro-mechanical perturbation. Illite was stable in comparison to montmorillonite, for which a new spacing was detected after the loading finished. This new spacing was also observed for *ex-situ* remoulded samples of sensitive clay, indicating a permanent change in fabric. During hydro-mechanical loading the two minerals continued to align towards the horizontal axis, as expected for a 1D compression test on a clay from a vertical borehole.

The initial principal orientation and degree of directional anisotropy, however, was markedly different for the two minerals.

The nano-scale scattering data was complemented with unique 3D image data on an undisturbed (saturated) sample of sensitive clay. The high spatial resolution with voxel size of 25 nm attained at a nanotomography beamline provides, for the first time, the internal 3D structure within the clay sample. The role of non-active particles, such as silt, in the mesoscale fabric was revealed, down to sub-µm scale. Strongly elongated particles larger than 2 µm and nano-grains with a small surface area entangled within the finer fractions in the sensitive clay investigated. The finer clay fraction could not be distinguished even at this scale, indicating that this sensitive clay has a large fraction of nanoparticles. *In-operando* triaxial compression tests were conducted, in order to exploit X-ray imaging as a very accurate 3D deformation gauge to obtain time-resolved internal deformations, *i.e.* 4D deformations, during hydro-mechanical probing of the sensitive clay. The low loading rate necessary for drained loading allowed continuous scanning, without pausing the test. Moreover, the absorption contrast offered by larger particles naturally embedded in the sensitive clay gave an unique opportunity to use a laboratory tomograph. Tomography measurements were acquired at several time instances during three separate tests with different stress ratios, highly deviatoric, $K_0$ and pseudo-isotropic ($\eta$=0.90, $\eta$=0.55 and $\eta$=0.18). DVC was used to extract 4D deformations, i.e. volumetric and deviatoric strains, from the tomography data.

The mean values of the full-field strain fields compare reasonably well with the external measurements at the sample boundary of axial displacement and volume change (volume of expelled pore water), with the best match for the $K_0$ stress path. These findings reinforce the validity of prior experimental data on soft clays that are based on boundary level measurements. Furthermore, the ratio of the deviatoric and mean effective stress measured at boundary value level is compared to the local evolution of the deviatoric and volumetric strain increments. The ratio of deviatoric and volumetric strain increments exhibits near bi-linear behaviour, and stabilises at large values of total strain. The most homogeneous full field strain maps are for the test with the $K_0$ stress path, whereas the test performed with a high $\eta$ ratio, involving intense shearing, resulted in the most inhomogeneous response.

The real-time monitoring using X-ray scattering and/or XCT during plane strain oedometer and drained triaxial tests demonstrate that geomechanical laboratory experiments on fine-grained soils can be elegantly combined with non-destructive techniques, to complement the data gathered by hydro-mechanical probing.

## 4.2 Recommendations

The work presented in this thesis is a first step towards *in-operando* monitoring of natural fine-grained soils in their intact state through all the relevant length scales. A natural extension would be to combine multiple techniques to simultaneously capture the material response at different length scales for the same deforming sample. An example of this is the combined use of XRD and XCT that is becoming available at an increasing number of beamlines. This would offer a holistic interpretation of the

mechanisms that occur during hydro-mechanical loading of natural fine-grained soils. Still a complex and challenging task is to acquire unbiased and high-quality 3D image data for the finest fraction of clay particles, to assess the theories about the transition of the structure of natural clays (*e.g.*, honeybomb, cardhouse). The sub-µm scale, which such structures exhibit, is close to the limit of the current capabilities of X-ray imaging. In this study, primarily a natural sensitive clay has been studied as benchmark material, as well as kaolin mixtures as a clay proxy. The complex composition of the natural clay complicated the interpretation of (especially) the scattering data. It would be beneficial to simplify the material complexity, whilst retaining some of the features observed in natural clays, such as well characterised synthetic clay systems (Fossum, 1999) with large particle inclusions. Finally, the role of the adsorbed water and the flow of the free water in the pore system is important in the emerging hydro-mechanical response of fine-grained soils at continuum scale. In the present study, the aim was to minimise the influence from the generation and dissipation of excess pore water pressures by choosing the loading rate to be sufficiently low to allow the pore water to drain from the sample. Still, the generation of (localised) pore water pressures forms an important aspect in the response of saturated fine-grained soils, and should be studied in more detail. In addition to using X-ray based measurement techniques, equivalent neutron source based methods that are more sensitive to water should be considered for the study of mineral-water surfaces, such as (quasi-elastic) neutron scattering (Ross et al., 2009; Swenson et al., 2000). Neutron imaging could be considered as well, however, at present it does not resolve submicron spatial features. Furthermore, the neutron attenuation in water is high, mandating small clay samples.

# Bibliography


Adrian, L., R.J. Adrian, and J. Westerweel (2011). *Particle image velocimetry*. Cambridge, UK: Cambridge university press (cit. on p. 36).

Alshibli, K.A. and A. Hasan (2008). "Spatial variation of void ratio and shear band thickness in sand using X-ray computed tomography". In: *Géotechnique* 58.4, pp. 249–257 (cit. on pp. 5, 31).

Amavasai, A., N. Sivasithamparam, J. Dijkstra, and M. Karstunen (2018). "Consistent Class A & C predictions of the Ballina test embankment". In: *Computers and Geotechnics* 93, pp. 75–86 (cit. on p. 3).

Andò, E. (2013). "Experimental investigation of microstructural changes in deforming granular media using x-ray tomography". PhD thesis. Université de Grenoble (cit. on p. 5).

Andò, E., R. Cailletaud, E. Roubin, O. Stamati, and the spam contributors (2017–). *spam: The Software for the Practical Analysis of Materials*. `https://ttk.gricad-pages.univ-grenoble-alpes.fr/spam/` (cit. on p. 39).

Andò, E., S.A. Hall, G. Viggiani, D. Desrues, and P. Bésuelle (2012). "Grain-scale experimental investigation of localised deformation in sand: a discrete particle tracking approach". In: *Acta Geotechnica* 7.1, pp. 1–13 (cit. on pp. 5, 31).

Andò, E., E. Salvatore, J. Desrues, P. Charrier, J-B. Toni, G. Modoni, and G. Viggiani (2017). "Strain localisation in sand in cycles of triaxial compression and extension: continuum and grain-scale analysis". In: *Papamichos E., Papanastasiou P., Pasternak E., Dyskin A. (eds) Bifurcation and Degradation of Geomaterials with Engineering Applications. IWBDG 2017. Springer Series in Geomechanics and Geoengineering*. Springer, Cham (cit. on p. 31).

Atterberg, A. (1911). "Die plastizität der tone". In: *Internationale Mitteilungen für Bodenkunde* 1 (1), pp. 10–43 (cit. on p. 7).

Auweter, S.D., J. Herzen, M. Willner, S. Grandl, K. Scherer, F. Bamberg, M. F. Reiser, F. Pfeiffer, and K. Hellerhoff (2014). "X-ray phase-contrast imaging of the breast—advances towards clinical implementation". In: *The British Journal of Radiology* 87.1034, p. 20130606. DOI: `10.1259/bjr.20130606` (cit. on p. 24).

Barnes, H.A. (1997). "Thixotropy-a review". In: *J. Non-Newtonian Fluid Mech.* 70, pp. 1–33 (cit. on p. 18).

Beckwith, T.G., R.D. Marangoni, and J.H.V Lienhard (2009). *Mechanical measurements*. Pearson (cit. on p. 36).

Bennet, R.H. and M.H. Hulbert (1986). "Concepts of clay fabric". In: *Clay Microstructure*, pp. 47–103 (cit. on p. 14).

Bergsten, H. (1994). "A high-resolution record of Lateglacial and early Holocene marine sediments from southwestern Sweden; with special emphasis on environmental changes close to the Pleistocene-Holocene transition and the influence of fresh water from the Baltic basin". In: *Journal of Quaternary Science* 9.1, pp. 1–12 (cit. on p. 3).

Bishop, A.W. and L.D. Wesley (1975). "A hydraulic triaxial apparatus for controlled stress path testing". In: *Géotechnique* 25.4, pp. 657–670 (cit. on p. 32).

Bitter, R., T. Mohiuddin, and M. Nawrocki (2006). *LabVIEW: Advanced programming techniques*. Crc Press (cit. on p. 33).

Bohor, B.F. and R.E. Hughes (1971). "Scanning Electron Microscopy of clay and clay minerals". In: *Clays and Clay Minerals* 19, pp. 49–54 (cit. on pp. 4, 14).

Bolt, G.H. (1956). "Physico-chemical analysis of the compressibility of pure clays". In: *Géotechnique* 6.2, pp. 86–93 (cit. on p. 16).

Brindley, G.W. and S.S Kurtosi (1962). "Quantitative determination of Kaolinite by X–ray diffraction". In: *The American Mineralogist* 47, pp. 1213–1215 (cit. on p. 4).

BS 5930 (1999). *Code of practice for site investigations*. Standard. London, UK: British Standards Institution (cit. on p. 16).

Cabrera, J.G. and I.J. Smalley (1973). "Quickclays as products of glacial action: a new approach to their nature, geology, distribution and geotechnical properties". In: *Engineering Geology* 7 (2), pp. 115–133 (cit. on p. 30).

Cartz, l. (1995). *Nondestructive Testing*. Ohio: ASM International (cit. on pp. 22, 26).

Casagrande, A. (1932). "Research on the Atterberg limits of soil". In: *Public Roads* 13, pp. 121–136 (cit. on p. 7).

Cloetens, P., W. Ludwig, J. Baruchel, D. Van Landuyt, J.P. Guigay, and M. Schlenker (1999). "Holotomography: Quantitative phase tomography with micrometer resolution using hard synchrotron radiation X–rays". In: *Appl. Phys. Lett.* 75, pp. 2912–2914. DOI: https://doi.org/10.1063/1.125225 (cit. on p. 29).

Collins, K. and A. McGown (1974). "The form and function of microfabric features in a variety of natural soils". In: *Géotechnique* 24 (2), pp. 223–254 (cit. on p. 13).

Cotecchia, F. and R.J. Chandler (1997). "The influence of structure on the pre-failure behaviour of natural clay". In: *Géotechnique* 47.3, pp. 523–544 (cit. on pp. 4, 13).

Cotecchia, F., S. Guglielmi, F. Cafaro, and A. Gens (2019). "Characterisation of the multi-scale fabric features of high plasticity clays". In: *Géotechnique Letters* 9 (4), pp. 361–368 (cit. on p. 15).

Cruden, D.M. and D.J. Varnes (1996). *Landslide types and processes*. National Academy Press, Washington, DC: Transportation research board, special report 247 (cit. on p. 18).

Cygan, R.T., J-J. Liang, and A.G. Kalinichev (2004). "Molecular models of hydroxide, oxyhydroxide, and clay phases and the development of a general force field". In: *J. Phys. Chem. B* 108 (4), pp. 1255–1266 (cit. on p. 16).

Davalos, J.F., A. Chen, I. Ray, and J.R. Levan (2012). "Comprehensive study on using externally bonded FRP composites for the rehabilitation of reinforced concrete T-beam bridges". In: *J Infrastruct Syst* 18.2, pp. 89–102 (cit. on p. 9).

Deirieh, A. (2016). "From clay clurries to mudrocks: A Cryo-SEM investigation of the development of the porosity and microstructure". PhD thesis. Massachussets Institute of Technology (cit. on pp. 4, 15, 21).

Deirieh, A., I.Y. Chang, M.L. Whittaker, S. Weigand, D. Keane, J. Rix, J.T. Germaine, D. Foester, and P.B Flemings (2018). "Particle arrangements in clay slurries: The case against the honeycomb structure". In: *Applied Clay Science* 152, pp. 166–172 (cit. on pp. 15, 21).

Delage, P. and G. Lefebvre (1984). "Study of the structure of a sensitive Champlain clay and of its evolution during consolidation". In: *Canadian Geotechnical Journal* 21.1, pp. 21–35 (cit. on pp. 4, 14, 15).

Diamond, S. (1970). "Microstructure and pore structure of impact compacted clays". In: *Clays Clay Miner* 19.4, pp. 239–249 (cit. on pp. 4, 14).

Díaz-Rodríguez, J.A and J.C. Santamarina (1999). "Thixotropy: the case of Mexico city soils". In: *XI Panamerican Conf. on Soil Mech. and Geotech. Eng*, pp. 441–448 (cit. on p. 18).

Dijkstra, J. and W. Broere (2010). "New method of full-field stress analysis and measurement using photoelasticity". In: *Geotechnical Testing Journal* 33 (6), pp. 469–481 (cit. on p. 21).

DiMasi, E., J. O. Fossum, T. Gog, and C. Venkataraman (2001). "Orientational order in gravity dispersed clay colloids: A synchrotron x-ray scattering study of Na fluorohectorite suspensions". In: *Physical Review E* 64, p. 061704 (cit. on p. 15).

Donaghe, R., R. Chaney, and M. Silver (1988). *Advanced triaxial testing of soil and rock*. West Conshohocken, PA: ASTM International (cit. on p. 4).

Du, J., R.A. Pushkarova, and R.St.C. Smart (2009). "A cryo-SEM study of aggregate and floc structure changes during clay settling and raking processes". In: *International Journal of Mineral Processing* 93.1, pp. 66–72 (cit. on p. 12).

Ebrahimi, D., R.J-M. Pellenq, and A.J. Whittle (2016). "Mesoscale simulation of clay aggregate formation and mechanical properties". In: *Granular Matter* 18.3, p. 49 (cit. on p. 16).

Ebrahimi, D., A.J. Whittle, and R.J-M Pellenq (2014). "Mesoscale properties of clay aggregates from potential of mean force representation of interactions between nanoplatelets". In: *The Journal of Chemical Physics* 140.15, p. 154309 (cit. on p. 16).

Ehrenberg, P. (1918). *Die bodenkolloide: eine ergänzung für die üblichen lehrbücher der bodenkunde, düngerlehre und ackerbaulehre*. Theodor Steinkopff (cit. on p. 14).

EN ISO 14688-1 (2017). *Geotechnical investigation and testing - Identification and classification of soil - Part 1: Identification and description*. Tech. rep. CEN-CENELEC Management Centre: Rue de la Science 23, B-1040 Brussels: EUROPEAN COMMITTEE FOR STANDARDIZATION (cit. on p. 7).

EN ISO 17892-6:2017 (2017). *Fall cone test*. Tech. rep. Swedish Standards Institute (cit. on p. 18).

Feldkamp, L.A., L.C. Davis, and J.W. Kress (1984). "Practical cone-beam algorithm". In: *Journal of the Optical Society of America A* 1.6, pp. 612–619 (cit. on p. 34).

Fodil, A., W. Aloulou, and P.Y. Hicher (1997). "Viscoplastic behaviour of soft clay". In: *Géotechnique* 47.3, pp. 581–591. DOI: https://doi.org/10.1680/geot.1997.47.3.581 (cit. on p. 19).

Fossum, J.O. (1999). "Physical phenomena in clays". In: *Physica A: Statistical mechanics and its applications* 270 (1-2), pp. 270–277 (cit. on p. 43).

Gajo, A. and D. Muir Wood (2001). "A new approach to anisotropic, bounding surface plasticity: general formulation and simulations of natural and reconstituted clay behaviour". In: *International Journal for Numerical and Analytical Methods in Geomechanics* 25.3, pp. 207–241 (cit. on p. 3).

Gao, Q-F., M.Hattab, M. Jrad, J-M. Flereau, and P-Y. Hicher (2020). "Microstructural organization of remoulded clays in relation with dilatancy/contractancy phenomena". In: *Acta Geotechnica* 15, pp. 223–243 (cit. on p. 19).

Gillot, J.E. (1970). "Fabric of Leda clay investigated by optical, electron-optical, and X-ray diffraction methods". In: *Engineering Geology* 4.2, pp. 133–153 (cit. on pp. 4, 14, 15).

Graham, J., J.H.A. Crooks, and A.L. Bell (1983). "Time effects on the stress-strain behaviour of natural soft clays". In: *Géotechnique* 33.3, pp. 327–340 (cit. on p. 19).

Gras, J-P, N. Sivasithamparam, M. Karstunen, and J. Dijkstra (2018). "Permissible range of model parameters for natural fine-grained materials". In: *Acta Geotechnica* 13.2, pp. 387–398 (cit. on p. 3).

Grédiac, M. and F. Hild (2012). *Full-field measurements and identification in solid mechanics*. John Wiley & Sons (cit. on pp. 36, 37).

Gregersen, O. (1981). "Quick clay landslide in Rissa, Norway". In: *NGI Publication* 135, pp. 1–6 (cit. on p. 18).

Grim, R.E. (1953). *Clay Mineralogy*. New York: McGraw-Hill Book Company, Inc. (cit. on pp. 4, 8, 14).

Grimstad, G., S. Abate Degago, S. Nordal, and M. Karstunen (2010). "Modeling creep and rate effects in structured anisotropic soft clays". In: *Acta Geotechnica* 5.1, pp. 69–81. DOI: https://doi.org/10.1007/s11440-010-0119-y (cit. on pp. 3, 19).

Hall, S.A., M. Bornert, J. Desrues, Y. Pannier, N. Lenoir, G. Viggiani, and P. Bésuelle (2010). "Discrete and continuum analysis of localised deformation in sand using X-ray CT and volumetric digital image correlation". In: *Géotechnique* 60.5, pp. 315–322 (cit. on pp. 5, 31, 35).

Hall, S.A., R.C. Hurley, and J. Wright (2018). "Micromechanics of granular media characterised using X-Ray Tomography and 3DXRD". In: *Giovine P., Mariano P., Mortara G. (eds) Micro to MACRO Mathematical Modelling in Soil Mechanics.* Birkhäuser, Cham (cit. on pp. 6, 21).

Hashash, Y.M.A and A.J Whittle (1996). "Ground movement prediction for deep excavations in soft clay". In: *Journal of Geotechnical Engineering* 122 (6), pp. 474–486 (cit. on p. 3).

Hattab, M. and J-M. Fleureau (2010). "Experimental study of kaolin particle orientation mechanism". In: *Géotechnique* 60.5, pp. 323–331 (cit. on pp. 4, 15).

Hattab, M., T. Hammad, J-M. Fleureau, and P-Y Hicher (2013). "Behaviour of a sensitive marine sediment: microstructural investigation". In: *Géotechnique* 63.1, pp. 71–84 (cit. on pp. 4, 15).

Iñigo, A.C., D. Tessier, and M. Pernes (2000). "Use of X-ray Transmission Diffractometry for the study of clay-particle orientation at different water contents". In: *Clay and Clay Minerals* 48.6, pp. 682–692 (cit. on pp. 4, 15).

Işik Ece, Ö. and P.A. Schroeder (2007). "Clay mineralogy and chemistry of halloysite and alunite deposits in the Turplu area, Balikesir, Turkey". In: *Clays and Clay Minerals* 55.1, pp. 18–35 (cit. on p. 12).

Jakobsson, B. (1952). "Landslide at Surte on the Göta river." In: *Proceedings, vol. 5, Statens Geotekniska Institut*. (Visited on 09/12/2016) (cit. on p. 18).

Karstunen, M. and M. Koskinen (2008). "Plastic anisotropy of soft reconstituted clays". In: *Canadian Geotechnical Journal* 45, pp. 314–328. DOI: doi.org/10.1139/T07-073 (cit. on pp. 20, 31).

Karstunen, M., H. Krenn, S.J. Wheele, M. Koskinen, and R. Zentar (2005). "Effect of anisotropy and destructuration on the behavior of Murro test embankment". In: *International Journal of Geomechanics* 5.2, pp. 87–97 (cit. on p. 3).

Karstunen, M. and Z-Y. Yin (2015). "Modelling time-dependent behaviour of Murro test embankment". In: *Géotechnique* 60 (10), pp. 735–749 (cit. on p. 3).

Khaldoun, A., P. Moller, A. Fall, G. Wegdam, B. De Leeuw, Y. Méheust, J. O. Fossum, and D. Bonn (2009). "Quick clay and landslides of clayey soils". In: *Physical Review Letters* 103 (18), p. 188301. DOI: 10.1103/PhysRevLett.103.188301 (cit. on p. 18).

Khandal, R. and T.Tadros (1988). "Application of viscoelastic measurements to the investigation of the swelling of sodium montmorillonite suspensions". In: *Journal of Colloid and Interface Science* 125, pp. 122–128 (cit. on p. 14).

Lambe, T.W. and R.V. Whitman (1969). *Soil Mechanics*. New York: Wiley (cit. on pp. 4, 13).

Larsson, R. and M. Jansson (1982). *Landslide at Tuve November 30 1977*. Tech. rep. Linköping: Statens Geotekniska Institut (cit. on p. 3).

Larsson, R., G. Sällfors, P-E. Bengtsson, C. Alén, U. Bergdahl, and L. Eriksson (2007). *Skjuvhållfasthet- utv"ardering i kohesionsjord*. Tech. rep. Linköping: Statens Geotekniska Institut (cit. on p. 20).

Lefebvre, G. and D. LeBoeuf (1987). "Rate Effects And Cyclic Loading of Sensitive Clays". In: *Journal of Geotechnical Engineering* 113.5, pp. 476–489. DOI: 10.1061/(ASCE)0733-9410(1987)113:5(476) (cit. on p. 19).

Lenoir, N., M. Bornert, J. Desrues, P. Bésuelle, and G. Viggiani (2007). "Volumetric Digital Image Correlation Applied to X-ray Microtomography Images from Triaxial Compression Tests on Argillaceous Rock". In: *Strain* 43, pp. 193–205 (cit. on pp. 5, 31, 35).

Leroueil, S., M. Kabbaj, F. Tavenas, and R. Bouchard (1985). "Stress-strain-strain rate relation for the compressibility of sensitive natural clays". In: *Géotechnique* 35.2, pp. 159–180. DOI: https://doi.org/10.1680/geot.1985.35.2.159 (cit. on p. 19).

Lessard, C. and J. Mitchell (1985). "The causes and effects of aging in quick clays". In: *Canadian Geotechnical Journal* 22.3, pp. 335–346. DOI: https://doi.org/10.1139/t85-046 (cit. on p. 19).

L'Heureux, J.-S., S. Glimsdal, O. Longva, L. Hansen, and C. B. Harbitz (2011). "The 1888 shoreline landslide and tsunami in Trondheimsfjorden, central Norway". In: *Marine Geophysical Research* 32, pp. 313–329 (cit. on p. 3).

Li, Y., J. Dijkstra, and M. Karstunen (2018). "Thermomechanical Creep in Sensitive Clays". In: *J Geotech Geoenviron Eng* 144 (11), p. 04018085 (cit. on p. 19).

Lutterotti, L., M. Voltolini, H.R. Wenk, K. Bandyopadhyay, and T. Vanorio (2010). "Texture analysis of a turbostratically disordered Ca-montmorillonite". In: *American Mineralogist* 95.1, pp. 98–103. DOI: 10.2138/am.2010.3238 (cit. on p. 11).

Martin, R.T and C.C Lad (1975). "Fabric of consolidated kaolinite". In: *Clays and Clay Minerals* 23, pp. 17–25 (cit. on pp. 4, 15).

Matsushima, T., K. Uesugi, T. Nakano, and A.Tsuchiyama (2010). "Visualization of grain motion inside a triaxial specimen by micro X-ray CT at SPring-8". In: *Advances in X-ray tomography for Geomaterials*. John Wiley & Sons, Ltd, pp. 255–261 (cit. on pp. 5, 31).

Mitchell, J.K. and K. Soga (2005). *Fundamentals of soil behavior*. 3rd ed. John Wiley & Sons (cit. on pp. 7–10, 12, 18).

Mojid, M.A. (2014). "Diffuse Double Layer (DDL)". In: *Encyclopedia of Earth Sciences Series*, pp. 213–214 (cit. on p. 15).

Mouzon, J., I.U. Bhuiyan, and J.Hedlund (2016). "The structure of montmorillonite gels revealed by sequential cryo-XHR-SEM imaging". In: *Journal of Colloid and Interface Science* 465, pp. 58–66 (cit. on p. 13).

Muir Wood, D. (2004). *Geotechnical Modelling*. Oxfordshire, UK: Spon Press (cit. on p. 32).

Muir Wood, D. and G.V. Kumar (2000). "Experimental observations of behaviour of heterogeneous soils". In: *Mech.Cohes.-Frict.Mater.* 5.5, pp. 373–398. DOI: 10.1002/1099-1484(200007)5:5<373::AID-CFM100>3.0.CO;2-D (cit. on p. 17).

Nadeau, P.H (1985). "The physical dimensions of fundamental clay particles". In: *Clay minerals* 20, pp. 499–514 (cit. on p. 11).

Nadim, F., S.A.S. Pedersen, P. Schmidt-Thomé, F. Sigmundsson, and M. Engdahl (2008). "Natural hazards in Nordic countries". In: *Episodes* 31.1, pp. 176–184 (cit. on p. 3).

O'Brien, N.R (1971). "Fabric of Kaolinite and Illite floccules". In: *Clay and Clay Minerals* 19, pp. 353–359 (cit. on p. 15).

Olsson, M. (2013). "On Rate-Dependency of Gothenburg clay". PhD thesis. Chalmers University of Technology (cit. on p. 20).

Osterman, J. (1963). "Studies on the properties and formation of quick clays". In: *Clays and Clay Minerals* 12.1, pp. 87–108 (cit. on p. 18).

Paganin, D., S. C. Mayo, T. E. Gureyev, P. R. Miller, and S. W. Wilkins (2002). "Simultaneous phase and amplitude extraction from a single defocused image of a homogeneous object". In: *Journal of Microscopy* 206 (1), pp. 33–40 (cit. on pp. 28, 29).

Park, S.-J. and M.-K. Seo (2011). "Chapter 1 - Intermolecular Force". In: *Interface Science and Technology* 18, pp. 1–57 (cit. on p. 16).

Pestana, J.M. and A.J. Whittle (1999). "Formulation of a unified constitutive model for clays and sands". In: *International Journal for Numerical and Analytical Methods in Geomechanics* 23.12, pp. 1215–1243 (cit. on p. 3).

Petterson, K.E. (1955). "The Early History of Circular Sliding Surfaces". In: *Géotechnique* 5 (4), pp. 275–296 (cit. on p. 3).

Pusch, R. (1970). "Clay microstructure. A study of the microstructure of soft clays with special reference to their physical properties." In: *Proceedings No. 24* (cit. on p. 15).

Quigley, R.M. and C.D. Thompson (1966). "The Fabric of Anisotropically Consolidated Sensitive Marine Clay". In: *Can. Geotech. J.* 3.2, pp. 61–73 (cit. on pp. 4, 14).

Rosenqvist, I. TH. (1953). "Considerations on the Sensitivity of Norwegian Quick-Clays". In: *Géotechnique* 3.5, pp. 195–200. DOI: https://doi.org/10.1680/geot.1953.3.5.195 (cit. on p. 19).

Rosenqvist, I. Th. (1966). "Norwegian research into the properties of quick clay-A review". In: *Engineering Geology* 1.6, pp. 445–450 (cit. on p. 19).

Ross, N.L., E.C. Spencer, A.A. Levchenko, A.I. Kolesnikov, D.J. Wesolowski, D.R. Cole, E.Mamontov, and L. Vlcek (2009). "Studies of Mineral–Water Surfaces". In: *Liang L., Rinaldi R., Schober H. (eds) Neutron Applications in Earth, Energy and Environmental Sciences. Neutron Scattering Applications and Techniques.* Springer, Boston, MA (cit. on p. 43).

Rouainia, M. and D. Muir Wood (2000). "A kinematic hardening constitutive model for natural clays with loss of structure". In: *Géotechnique* 50.2, pp. 153–164 (cit. on p. 3).

Rubensson, J-E. (2016). "Synchrotron radiation". In: Morgan & Claypool Publishers. Chap. 6, pp. 1–20. DOI: http://dx.doi.org/10.1088/978-1-6817-4115-4ch6 (cit. on p. 22).

Rueden, C.T., J. Schindelin, M.C. Hiner, B.E. DeZonia, A.E. Walter, E.T. Arena, and K.W. Eliceiri (2017). "ImageJ2: ImageJ for the next generation of scientific image data". In: *BMC Bioinformatics* 18 (cit. on p. 30).

Sällfors, G. (1975). "Preconsolidation pressure of soft, high-plastic clays". PhD thesis. Chalmers University of Technology (cit. on p. 19).

Santamarina, J. C. (2003). "Soil behavior at the microscale: particle forces". In: *Soil behavior and soft ground construction*, pp. 25–56 (cit. on p. 17).

Seed, H.B., R.J. Woodward, and R. Lundgren (1966). "Fundamental aspects of the Atterberg limits". In: *Journal of Soil Mechanics & Foundations Div* 92 (cit. on p. 7).

Sivasithamparam, N., M. Karstunen, and P. Bonnier (2015). "Modelling creep behaviour of anisotropic soft soils". In: *Computers and Geotechnics* 69, pp. 46–57 (cit. on pp. 3, 19).

Small, C. and R.J. Nicholls (2003). "A global analysis of human settlement in coastal zones". In: *Journal of coastal research*, pp. 584–599 (cit. on p. 3).

Söderblom, R. (1966). "Chemical aspects of quick-clay formation". In: *Engineering Geology* 1.6, pp. 415–431. DOI: https://doi.org/10.1016/0013-7952(66)90018-4 (cit. on p. 19).

Sridharan, A. and M.S. Jayadeva (1982). "Double layer theory and compressibility of clays". In: *Géotechnique* 32.2, pp. 133–144 (cit. on p. 16).

Środoń, J. (1999). "Illite group clay minerals". In: *Encyclopedia of Earth Science*, pp. 597–601 (cit. on pp. 10, 11).

Stojek, Z. (2002). "The electrical double layer and its structure". In: *Electroanalytical Methods, Guide to Experiments and Applications* (cit. on p. 15).

Sutton, M.A., J.J. Orteu, and H. Schreier (2009). *Image correlation for shape, motion and deformation measurements: basic concepts, theory and applications*. Springer Science & Business Media (cit. on p. 36).

Svanström, S. (2012). "Varannan svensk bor nära havet". In: *Välfärd* 2, pp. 10–12 (cit. on p. 3).

Swenson, J., R. Bergman, and W.S. Howells (2000). "Quasielastic neutron scattering of twodimensional water in a vermiculite clay". In: *J. Chem. Phys.* 113, p. 2873 (cit. on p. 43).

Takano, D., N. Lenoir, J. Otani, and S. Hall (2015). "Localised deformation in a wide-grained sand under triaxial compression revealed by X-ray tomography and digital image correlation". In: *Soils and Foundations* 55.4, pp. 906–915 (cit. on p. 35).

Tarantino, A. and E. De Col (2008). "Compaction behaviour of clay". In: *Géotechnique* 58.3, pp. 199–213 (cit. on pp. 4, 14).

Tavenas, F., S. Leroueil, P. La Rochelle, and M. Roy (1978). "Creep behaviour of an undisturbed lightly overconsolidated clay". In: *Can. Geotech. J.* 15.3, pp. 402–423. DOI: https://doi.org/10.1139/t78-037 (cit. on p. 19).

Torrance, J.K. (1976). "Pore water extraction and the effect of Sample Storageon the pore water chemistry of Leda Clay". In: *Soil Specimen Preparation for Laboratory Testing, ASTM STP 599, American Society for Testing and Materials*, pp. 147–157 (cit. on p. 19).

Torrance, J.K. (1983). "Towards a general model of quick clay development". In: *Sedimentology* 30.4, pp. 547–555. ISSN: 1365-3091. DOI: 10.1111/j.1365-3091.1983.tb00692.x (cit. on p. 18).

Tudisco, E., S.A Hall, E.M. Charalampidou, N. Kardjilov, A. Hilger, and H. Sone (2015). "Full-field measurements of strain localisation in sandstone by neutron tomography and 3D-volumetric digital image correlation". In: *Physics Procedia* 69, pp. 509–515 (cit. on p. 37).

Underwood, T., V Erastova, and H. C. Greenwell (2012). "Wetting Effects and Molecular Adsorption at Hydrated Kaolinite Clay Mineral Surfaces". In: *J. Phys. Chem. C* 120.21, pp. 11433–11449 (cit. on p. 10).

van Olphen, H. (1964). "Internal mutual flocculation in clay suspensions". In: *Journal of Colloid Science* 19, pp. 313–322 (cit. on pp. 13, 14).

Weber, L. (2016). "Iterative tomographic X-Ray phase reconstruction". PhD thesis. L'Institut National des Sciences Appliquées de Lyon (cit. on p. 29).

Wheeler, S.J., A. Häätänen, M. Karstunen, and M. Lojander (2003). "An anisotropic elastoplastic model for soft clays". In: *Canadian Geotechnical Journal* 40.2, pp. 403–418. DOI: 10.1139/t02-119 (cit. on pp. 3, 19, 20).

White, W.A. (1949). "Atterberg plastic limits of clay minerals". In: *American Mineralogist* 34 (7-8), pp. 508–512 (cit. on p. 7).

Wichtmann, T., K.H. Andersen, M.A. Sjursen, and T. Berre (2013). "Cyclic tests on high-quality undisturbed block samples of soft marine Norwegian clay". In: *Canadian Geotechnical Journal* 50 (4), pp. 400–412 (cit. on p. 17).

Wood, T. and M. Karstunen (2017). "Modelling the creep of deep foundations in soft Gothenburg clays". In: *European Journal of Environmental and Civil Engineering*. DOI: 10.1080/19648189.2017.1344146 (cit. on p. 3).

Yin, Z-Y, C.S. Chang, M. Karstunen, and P-Y. Hicher (2010). "An anisotropic elastic–viscoplastic model for soft clays". In: *International Journal of Solids and Structures* 47.5, pp. 665–677. DOI: https://doi.org/10.1016/j.ijsolstr.2009.11.004 (cit. on p. 19).

Yin, Z-Y., M. Karstunen, C.S. Chang, M. Koskinen, and M. Lojander (2011). "Modeling Time-Dependent Behavior of Soft Sensitive Clay". In: *Journal of Geotechnical and Geoenvironmental Engineering* 137.11, pp. 1103–1113. DOI: 10.1061/(ASCE)GT.1943-5606.0000527 (cit. on p. 3).

Żbik, M.S. (2010). "Kaolinite platelet orientation for XRD and AFM applications". In: *Applied Clay Science* 50.3, pp. 229–304 (cit. on p. 11).

Zhao, D., Q-F. Gao, M. Hattab, P-Y. Hicher, and Z-Y. Yin (2020). "Microstructural evolution of remolded clay related to creep". In: *Transportation Geotechnics* 24, p. 100367 (cit. on p. 19).

Zhou, S. and A. Brahme (2008). "Development of phase-contrast X-ray imaging techniques and potential medical applications". In: *Physica Medica* 24.3, pp. 129–148 (cit. on p. 36).

Zhu, J-G. and J-H. Yin (2000). "Strain-rate-dependent stress–strain behavior of overconsolidated Hong Kong marine clay". In: *Can. Geotech. J.* 37.6, pp. 1272–1282. DOI: https://doi.org/10.1139/t00-054 (cit. on p. 19).